Article

Heat-Up Performance of Catalyst Carriers – A Study of Urban Drive Cycles

Thomas Steiner , Verena Schallhart , Luca Nohel , Philipp Pichler , Martin Wilhelm , Christoph Pfeifer , Lukas Möltner *

Posted Date: 23 April 2026

doi: 10.20944/preprints202604.1657.v1

Keywords: catalytical converter; cell density; cordierite; emission control; electrical heating; hybrid ceramic; light-off; monolith; wall thickness

 doi:10.20944/preprints202604.1657.v1

Article

Heat-Up Performance of Catalyst Carriers – A Study of Urban Drive Cycles

Thomas Steiner [1,2], Verena Schallhart [2], Luca Nohel [2], Philipp Pichler [2], Martin Wilhelm [2], Christoph Pfeifer [1] and Lukas Möltner [2,*]

[1] University of Natural Resources and Life Sciences, Institute for Chemical and Energy Engineering

[2] Management Center Innsbruck, Department for Industrial Engineering and Management

* Correspondence: lukas.moeltner@mci.edu; Tel.: +43 512 2070 4132

Abstract

This study investigates the geometric parameters of commercially available or recently published models of catalyst substrates for passenger vehicles and provides a numerical evaluation of their influence on thermal behavior for use in urban areas. To ensure the plausibility of the results, a range of scenarios have been meticulously designed to replicate real operational conditions. To ensure a reliable basis for comparison, all geometries were standardized to the same gas-solid exchange surface by adapt the total monolith length. The simulation experiments conducted revealed that the primary role in question is played by the mass of the monolith and its internal surface area, while the heat transfer coefficient plays a secondary role. The necessity of adapting the geometry to the deployment scenario was demonstrated by comparing the performance of different scenarios. The employment of contemporary technologies, such as start-stop systems and automatic catalytic converter preconditioning, has also been factored. The study's findings suggest that geometries characterized by high cell density and low wall thickness, in conjunction with modern materials and intelligent engine control, are ready to become the norm for future ICE applications. This claim is particularly salient in the context of the requirements of mobile exhaust gas purification systems.

Keywords: catalytical converter; cell density; cordierite; emission control; electrical heating; hybrid ceramic; light-off; monolith; wall thickness

1. Introduction

Catalytic converters are indispensable in improving emission treatment efficiency and reducing the environmental footprint of internal combustion engines (ICE), irrespective of their purpose. They enable the conversion of harmful exhaust gas components into less toxic substances under given conditions, making them a cornerstone of modern emission control. However, the thermal challenges associated with mobile systems significantly limit catalyst's performance, durability, and cost-effectiveness. Mobile applications frequently expose catalysts to rapid thermal cycling and sustained high-temperature operations, which accelerate deactivation processes such as sintering, thermal aging, and phase transformations of the catalytical material.

A significant thermal issue in mobile applications, particularly in the automotive sector, is the achievement of the catalyst's light-off temperature. This is defined as the minimum temperature at which the catalyst achieves a conversion rate of 50 %. Cold-start conditions, which are prevalent in short trips and urban driving, delay the attainment of this threshold, resulting in disproportionately high emissions during the initial phase of engine operation. This problem is further compounded by increasingly stringent emissions regulations, such as Euro VII in Europe and Tier 3 in the United States [1,2]. These impose strict limits on total emissions, including those produced during real-driving conditions. The main challenge is the design of a catalysts that can swiftly reach and maintain the light-off temperature, even under adverse thermal and operational conditions, without compromising long-term durability. All of the future standards are focusing on a reduction of

 doi:10.20944/preprints202604.1657.v1

nitrogen oxides (NO_x), particulate matter (PM), and unburned hydrocarbons (C_xH_y), with a concomitant emphasis on the real-driving emissions (RDE).

Addressing these challenges necessitates a multi-disciplinary approach, integrating advances in catalyst material science, enhanced thermal management techniques, and innovative system designs. The present study investigates the nature of thermal issues in catalysts for mobile applications, with a particular focus on the light-off temperature. It also evaluates current strategies for pass these challenges and proposes pathways to develop thermally robust catalyst technologies capable to meet future regulatory demands.

2. Problem Statement and Scope of this Study

Regardless of the type of catalytic converter in question, it is an essential prerequisite that a specific minimum operating temperature is attained. Below this critical limit, the conversion efficiency for pollutants remains low, leading to elevated emission levels. Within the context of catalytic converter functionality, two fundamental challenges emerge. The first of these is the minimization of the time from engine start-up to reaching the light-off temperature. The second challenge pertains to the necessity of maintaining the converter's temperature above this level during unfavorable operating conditions, such as idling phases.

These challenges have become increasingly significant with the introduction of more stringent emissions regulations in all industrial countries worldwide. The forthcoming EURO VII standards [1], effective from the end of 2026 for new vehicle models in Europe, will further tighten the regulatory screws. In addition to the regulations introducing controls on particulate emissions, including particles as small as 10 nm, these regulations will enforce stricter compliance tests under real driving conditions, ranging from - 10 °C to 45 °C ambient temperature. This underscores the critical need to optimize light-off performance and maintain catalyst efficiency to meet these rigorous standards while achieving reduced environmental impacts. A significant addition due to the legislation is the requirement for enhanced system durability. The provision stipulates that emission control systems must now ensure compliance with pollutant limits for a minimum of ten years or 200,000 km, a substantial extension compared to previous standard. This measure is designed to ensure consistent emission reductions throughout the vehicle's operational life.

The integration of multiple catalytic converters within a state-of-the-art exhaust system is imperative to ensure the attainment of requisite emission limits. Each catalytic converter functions as a thermal mass, thereby impacting the subsequent gas temperature within the exhaust system. Consequently, catalytic converters exert a dampening effect on the transient temperature curve of the ICE. It is noteworthy that the initial catalytic converter plays a pivotal role, as it is most effected of all units in the exhaust gas stream. With regard to the light-off temperatures, the diesel engine is of particular noted, as the exhaust gas temperatures are generally lower than those of an petrol engine.

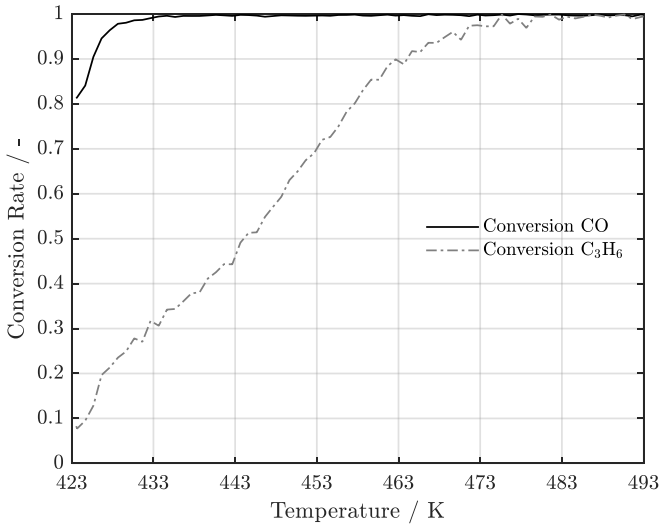

 doi:10.20944/preprints202604.1657.v1

Figure 1. Experimental determined conversion rates of a 3:1:0 (Pt:Pd:Rh) DOC for oxidizing CO and C_3H_6.

As shown in Figure , the conversion curves of a diesel oxidation catalyst (DOC) containing platinum, palladium and rhodium in a ratio of 3:1:0 (Pt:Pd:Rh) are presented. The catalytic converter has a washcoat loading of 40 g ft^{-3} and was hydrothermally aged for 16 h at 750 °C in the presence of 10 % water (H_2O) in synthetic air (SynAir). Conversion analysis was performed at 50,000 h^{-1} with a synthetic gas containing 10 % H_2O, 10 % carbon dioxide (CO_2), 6 % oxygen (O_2), 500 ppm nitrogen monoxide (NO), 150 ppm carbon monoxide (CO) and 50 ppm propene (C_3H_6), balanced with SynAir.

The abscissa represents the temperature and the ordinate the conversion rate. The conversion curve of C_3H_6 is indicative of unburnt hydrocarbons, which necessitate a higher oxidation temperature in comparison to CO. The utilization of aged catalytic converter data is a fundamental aspect of this study, as it aligns with a realistic fleet in operation and incorporates the critical consideration that the systems must continue to adhere to stringent emission limits even after an extended period of use.

The decisive factor when analyzing catalytic converters is the achievement of a conversion rate of 50 %. This value is critical for determining the light-off temperature, which is achieved at approx. 444 K in this case. Consequently, this study utilizes the aforementioned value as the designated light-off temperature.

Addressing these issues, the study investigates the thermal behavior of catalytic converters by modelling the heat transfer processes between the exhaust gas and the converter. Through numerical simulations, the research evaluates the impact of various geometric and physical parameters on the thermal efficiency of the converter, with the ultimate goal of supporting decisions on optimal designs and heating strategies.

3. Literature Review

Initiatives aimed at reducing vehicle emissions have been in progress since the late 1960s. The establishment of the first statutory emission limits in the USA occurred in 1967 as part of the Federal Air Quality Act (FAQA) [3]. In Germany, the initial regulation of the Federal Imission Control Act (1.BlmSchV) [4] was implemented in 1974. Subsequent to that period, a series of increasingly stringent regulations pertaining to exhaust emission have been implemented. In order to comply with these regulations, car manufacturers have adopted various strategies.

3.1. Internal Measures

The configuration of engines and the conceptualization of combustion exert a substantial influence on the chemical reactions that transpire within the combustion chamber and the resultant emissions. In recent years, there has been a concerted effort to reduce CO_2 emissions. The primary factors influencing these metrics are fuel consumption and efficiency, with a focus on enhancing the utilization of fuel. A variety of concepts are employed to achieve this objective.

3.1.1. Direct Injection and Injection Timing

The efficacy of direct injection has been demonstrated in reducing fuel consumption, particularly in part-load operation. Consequently, this technology has become a staple in the design of modern engines. The process of fuel injection results in the atomization of the fuel, leading to the formation of a greater number of minute particles within the exhaust gas. Nevertheless, these phenomena give rise to substantial health concerns, particularly for individuals residing in close proximity. Consequently, particulate filters have become a prevalent component in contemporary vehicles, including both diesel and petrol engines.

The precise timing of the injection process is of the utmost importance for achieving optimal combustion efficiency. The element under consideration exerts a direct influence on the mixture formation, the resulting emissions, the exhaust gas temperature, and the knocking tendency

 doi:10.20944/preprints202604.1657.v1

(especially in gasoline use) of engines. Contemporary systems possess the capability to subdivide the injection into multiple events. Consequently, a three-part injection system, comprising a pilot, main, and post-injection component, is considered to be state-of-the-art. This facilitates the optimization of combustion processes with regard to NO_x formation, soot formation, noise generation, and combustion duration. In the context of gasoline engines, this phenomenon enables the occurrence of stratified combustion, wherein the fuel-air ratio can be achieved in a distinct manner at local versus global levels. Nonetheless, the enhanced efficiency is accompanied by elevated NO_x emissions. [5]

3.1.2. Exhaust Gas Recirculation (EGR)

The recirculation of a bypass flow of exhaust gas into the combustion chamber has been demonstrated to facilitate the modulation of the combustion process. It is generally accepted practice to cool the recirculated gas prior to its reintroduction into the combustion chamber. This process has been demonstrated to reduce combustion temperature and subsequently NO_x emissions. According to the extant research, a reduction in exhaust gas temperature gives rise to the carbon monoxide (CO) emissions. Furthermore, the presence of unburned hydrocarbons in exhaust gas was found to be more pronounced. Concurrently, the exhaust gas temperature is reduced, exerting a deleterious effect on the catalytic converters within the exhaust tract. This phenomenon is especially evident in the context of achieving and sustaining the target light-off temperature. [6]

3.1.3. Miller Cycle

The Miller cycle is frequently employed in contemporary vehicles, as it has the capacity to enhance efficiency, thereby reducing CO_2 emissions. The enhanced efficiency of this principle results in a reduction in combustion chamber temperature and exhaust gas temperature. As with EGR, this reduces NO_x but increases unburned hydrocarbons and CO emissions. [7]

The majority of contemporary internal engine measures are oriented towards enhancing efficiency and, consequently, reducing CO_2 emissions. A select number of these systems have been demonstrated to reduce NO_x emissions; however, only a limited number have been shown to reduce unburned hydrocarbons or CO emissions.

3.2. Passive External Measures

The internal engine measures to reduce emissions are directly related to all associated parameters. These include the combustion concept, engine geometries and engine control. Conversely, external engine measures address the exhaust gas emanating from the engine without exerting a direct influence on the combustion process and emission formation. Nevertheless, the impact of external units on exhaust back pressure and pressure loss within the exhaust system must be taken into account. This has a significant influence on the parameters of the turbocharger and thus also directly on all other combustion parameters. Consequently, the downstream units must also be adapted to the respective engine. With regard to the reduction of external emissions, a distinction can be made between active and passive measures.

3.2.1. Constructive Measures

In the context of a catalytic reaction, attaining the requisite reaction initiation temperature is of paramount importance. Positioning is a critical aspect of this process. Consequently, the catalysts are strategically positioned in close proximity to the engine, ensuring optimal structural integrity.

The exchange surface between the catalytic surface and the fluid plays an important role in heterogeneous catalysis. Consequently, a primary objective is to ensure an ample contact area. Concurrently, the requisite temperature must be present to attain the necessary activation energy. It is imperative to acknowledge the significance of the catalyst's mass in conjunction with its exchange surface. In addition to the factors influencing the reaction kinetics, the influence of the additional installations in the exhaust tract on the entire system must be considered. At this juncture that the

 doi:10.20944/preprints202604.1657.v1

supplementary pressure loss becomes salient. The magnitude of this loss is determined by the open frontal area (OFA). Consequently, this value must also be considered in the analysis. [8]

A preliminary investigation has demonstrated that a reduced wall thickness and diminished cell density exert a favorable influence on the OFA. The versions with 2 mil also demonstrated the optimal value. The discrepancy in wall thickness between 600 cpsi and 900 cpsi is small, with a variation of only 2.3 %. Consequently, the versions with a low wall thickness would be optimal in this regard, with the type with 2 mil and 600 cpsi achieving the most advantageous value among all the geometries evaluated. [9]

Concurrently, novel designs are being developed to amalgamate the requisite advantages. One such system that was developed here is the ring catalytic converter design. The design was developed for three-way catalytic converters (TWC) that are located in close proximity to the engine. [10]

3.2.2. Material Development

In addition to the design measures, the reaction on the catalyst itself is also crucial for the catalytic conversion of reactants. Consequently, there is ongoing research in this area to develop new materials that can reduce the required light-off temperatures, increase the loadings, and also develop more cost-effective materials. Aging processes have been identified as a primary factor influencing catalytic activity. Consequently, they have become the focal point of numerous research initiatives. [11]

3.3. Active External Measures

Passive measures are designed to maximize the use of the available thermal energy in the exhaust gas to create the necessary operating conditions for the aftertreatment systems. Active systems, on the other hand, directly influence the heat balance.

3.3.1. Electric Heating Systems

The use of electric heating systems for catalytic converters in mobile ICE applications is gaining momentum. In recent years, the use of 48-volt printed circuit boards has become increasingly common as the sophistication of on-board systems has increased. This shift represents a departure from the previous standard of 12-volt boards and indicates a move towards more advanced and complex electrical systems. This configuration offers a significant advantage for electric heating systems, as it allows the required amperage to be reduced by a quarter while maintaining the same electrical output. It is also possible to connect an electric preheater upstream of the catalyst to increase the exhaust gas temperature. It is important to note that the entire catalyst can also be heated. To date, metallic catalyst substrates have been the dominant technology in this area. However, recent research has shifted towards the exploration of ceramic alternatives that possess electrical conductivity and thus allow for direct heating [12]. The use of microwave radiation as a means of heating the catalyst is also a possibility.

3.3.2. Fuel Burner

Instead of electrical heating, burners are also considered as a means to quickly reach the required light-off temperature, especially during cold starts. In this scenario, a modest amount of the fuel available in the vehicle is used to directly heat the catalysts immediately after the engine is started. This is also referred to as a catalytic burner. The additional fuel consumption has a negative effect on overall CO_2 emissions, even if it reduces other emissions. [13]

So far, active measures have not been used as standard practice for passenger cars, but this is expected to change with the implementation of the EURO VII standards. At present, it is not possible to predict which system will prevail in the market.

 doi:10.20944/preprints202604.1657.v1

4. Methodology

This section provides an overview of the chronological sequence of investigations. In an earlier published study examined the thermal behavior of catalytic converters, focusing on the influence of geometric parameters [9]. Variables such the mass, the area of contact between the gas and the catalyst, or the free surface area were systematically varied and subjected to detailed analysis. The study revealed that the geometric parameters, specifically cell density and wall thickness, exert a significant influence on the thermal behavior of the catalysts. In the initial phase, the impact of geometric parameters on the physical characteristics of the monolith was examined. Subsequently, the extent to which geometric properties influence thermal processes was investigated. The analysis was illustrated and compared using a load step. The representation of a load step provides information about the thermal behavior of a geometry in the event of heating or cooling, which is important for reaching a target temperature, but not the behavior under changing input conditions. This means that while the heating phase can be mapped, the question of whether the desired temperature can be maintained during operation remains unanswered.

This work therefore goes an important step further and simulates a real measured driving cycle. The determination of a typical load case within an urban area is achieved through test driving, which serves the starting point for the subsequent simulation of catalytic converter temperatures. Furthermore, the impact of an automatic start-stop system and supplementary electrical heating is also considered.

In the context of the present study, commercially available standards were selected for the honeycomb catalysts. The reference dimension has a diameter of 5.66 in (0.144 m) and a length of 6.0 in (0.152 m). To facilitate a comparison between different geometries, the cell density and the associated wall thickness are varied. The monolith employed as the standard for comparison has a cell density of 400 cpsi (cells per square inch) ($6.2 \cdot 10^5$ cells per m^2) and a wall thickness of 4 mil ($1.02 \cdot 10^{-4}$ m). The selection of monoliths under consideration is based on an earlier published study, as displayed in Table [9]. The geometry with 400 cpsi and 4 mil is utilized as a reference for all subsequent considerations.

Due to the widespread use of non-metric units in the context of describing monoliths' dimensions and to ensure the comparability to other surveys, this study remains consistent with pertinent literature.

Table 1. Overview of the investigated honeycomb geometries.

Geometry	300 cpsi	400 cpsi	600 cpsi	750 cpsi	900 cpsi	1200 cpsi
2 mil	-	-	x	x	x	x
3 mil	-	x	x	-	-	-
4 mil	-	x	x	-	-	-
6 mil	x	x	-	-	-	-
8 mil	x	-	-	-	-	-

4.1. Experimental Data Acquisition

In order to measure real driving data, test drives were carried out within the urban area of Innsbruck. It is noteworthy that the resultant speed range is, closely aligned with the low-speed segment of the WLTP. The test was conducted using an EURO V emission class vehicle, with additional data provided in

 doi:10.20944/preprints202604.1657.v1

Table . The average age of vehicles in Austria and Germany is just about ten years, meaning that this vehicle represents a typical cross-section of the current vehicle fleet [14].

 doi:10.20944/preprints202604.1657.v1

Table 2. Summary of the test vehicle's basic data.

Manufacturer	Skoda
Model	Octavia
Year of manufacture	2015
Emission standard	EURO V
Number of cylinders	4
Operating principle	Four-Stroke-Diesel
Engine displacement	1598 ccm³
Vehicle weight	1381 kg
Power output	77 kW (@4000 rpm)

Three test drives were conducted with the objective of ascertaining the requisite measurement data. It is noteworthy that all three runs were initiated with a cold engine start. The initial two drives were executed with the start-stop system enabled, while the third drive was conducted with the system deactivated. This made it possible to determine the activation points of the idle stop system and also the values required for the engine to run at idle speed.

The data was collected using vehicle diagnostic software (moDiag), with a measurement interval of one second. The speed values were recorded with the assistance of an external Global Positioning System (GPS) system. The route followed by the GPS in the urban area of Innsbruck is illustrated in Figure and the speed profile in Figure .

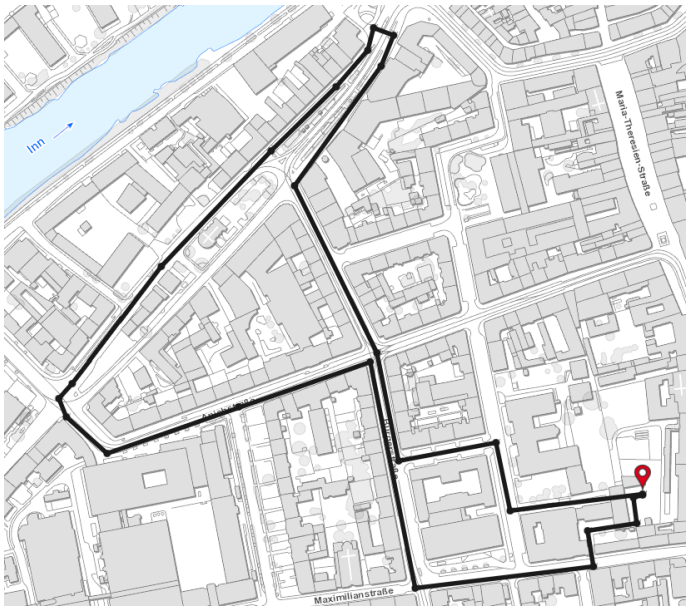

Figure 2. The route of the test drive has been documented through GPS tracking [15].

Due to the minimal altitude difference of only a few meters throughout the entire city of Innsbruck, the altitude profile of the test round is not shown separately. The data presented in the following diagrams are recorded on June 9 2020 at 04 p.m. local time. The ambient temperature was recorded with 16.4 °C, while air pressure was 100,990 Pa.

 doi:10.20944/preprints202604.1657.v1

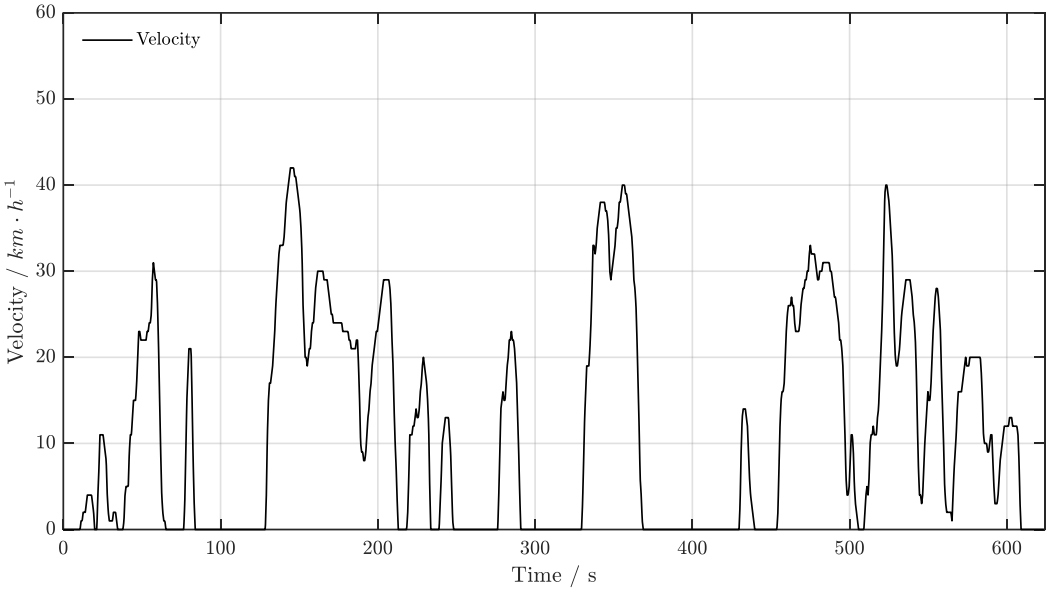

Figure 3. Velocity profile of the driving cycle.

In the context of urban areas, the velocity is characterized by high variability, with frequent interruptions of traffic stoppage due to traffic lights or intersections. Concurrently, the attained maximum velocity remains below the obligatory urban limit of 50 km h^{-1}. The speed curve reveals very short times of maximum speed and three extended idling periods.

The exhaust gas temperature is measured between the combustion engine and the DOC catalytic converter, with the resultant measurement being provided directly by the system. The exhaust gas mass flow must be calculated using the measured values of the injector control for the fuel volume flow. The quantity of fuel required is contingent upon the driving conditions, and is calculated by the injection control unit based on engine speed and load. The moDiag diagnostic software determines the expected fuel consumption based on the accelerator pedal position. The estimation of exhaust mass flow is achieved through the conversion of fuel volume flow into mass flow using the fuel density, as outlined in Equation (1).

$$\dot{m}_{fuel} = \dot{V}_{fuel} \cdot \rho_{fuel} \quad (1)$$

The temperature of the fuel was considered to be 16 °C and a density of 837 kg·m^{-3} was used for the calculation. The temperature values recorded by the diagnostic tool were subsequently interpolated in a time interval step of 0.2 s for further calculations. The exhaust mass flow was then calculated for all recorded values using Equation 2, based on the calculated fuel mass flow and the determined intake air mass flow.

$$\dot{m}_{exhaust} = \dot{m}_{fuel} + \dot{m}_{air} \quad (2)$$

The following diagram (Figure) is generated by utilizing the measured exhaust gas temperature and the calculated gas mass flow. Both values are represented graphically over time. It is important to note that this cycle was recorded with the start-stop system deactivated; consequently, the mass flow does not decrease to zero, even during extended periods of downtime.

 doi:10.20944/preprints202604.1657.v1

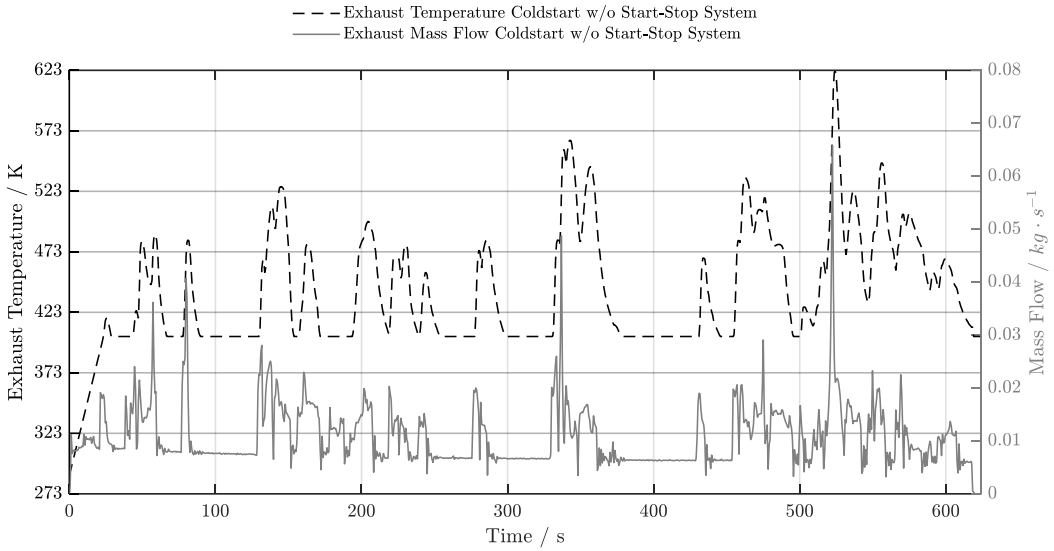

Figure 4. Exhaust gas temperature curve and exhaust gas mass flow curve for cold start w/o start-stop system.

4.2. Simulation Model

The simulation model of Moeltner et al. in [16] is used for the numerical investigation of the temperature behavior of automotive converters. The heat transfer processes in the exhaust gas system are calculated by two parallel running 1D simulations. The model incorporates the temperature changes in the catalyst, as well as the change in exhaust gas. The calculation of the temperature trend is achieved through the utilization of uniformly distributed cells throughout the exhaust system, as illustrated in Figure . The dimensions of these cells are chosen such that a further reduction in size would have negligible effect on the accuracy of the results. The model is validated by comparing the calculations and empirical data presented in [16].

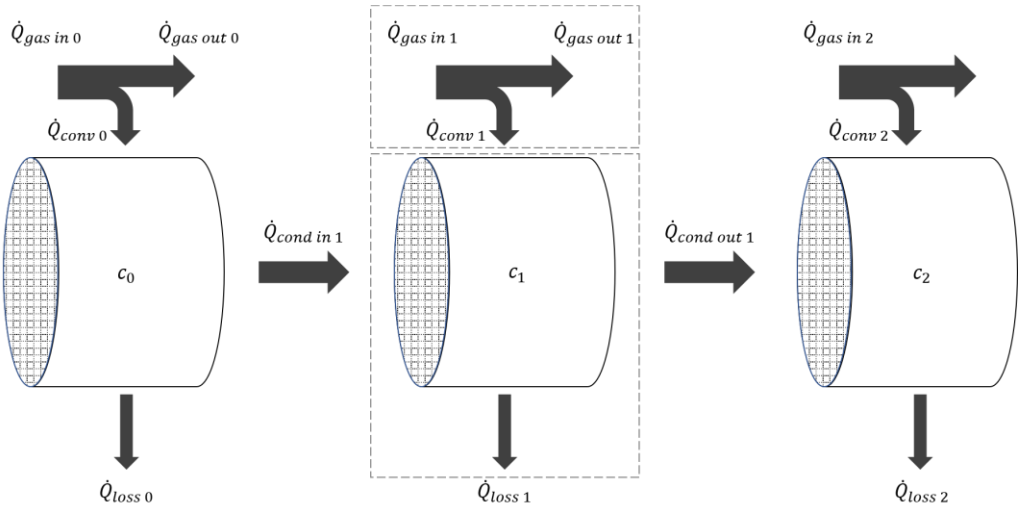

Figure 5. Illustration of the cell modelling of the calculation system.

A detailed study of a single cell shows that four different heat exchange processes take place. The subsequent Equation 3 encompasses all of these processes, the conductive heat transfer between the individual cells, the convective heat transfer between the exhaust gas and the after-treatment system, and the heat losses.

$$\dot{Q}_{conv} = m_{solid} \cdot c_{p_{solid}} \cdot \frac{dT}{dt} = \pm\dot{Q}_{cond\ in\ 1} \pm \dot{Q}_{conv\ 1} \pm \dot{Q}_{cond\ out\ 1} - \dot{Q}_{loss\ 1} \quad (3)$$

 doi:10.20944/preprints202604.1657.v1

The process of heat exchange between exhaust gas and catalytic converter material is predominantly governed by convection. The fundamental influencing factor is the temperature difference between the medium and the honeycomb body. Furthermore, the flow characteristics and the geometry of the contact surface are found to be the key determinants of heat transfer. Consequently, the exhaust gas and the catalyst surface undergo constant temperature fluctuations due to the perpetual exchange of heat. This implies that two temperature calculations are required, one for the gas and a second for the honeycomb.

$$\dot{Q}_{conv} = \dot{m}_{gas} \cdot c_{p\,gas} \cdot \Delta T_{gas} = \alpha \cdot A_{int} \cdot \Delta T_{\,ln\,mean} \tag{4}$$

The temperature development of the exhaust gas is governed by the heat emitted or absorbed within a gas cell due to forced convection between the exhaust gas and the after-treatment system. The temperature difference in the gas cell is estimated using the logarithmic mean temperature difference ($\Delta T_{\,ln\,mean}$), as demonstrated in Equation 4. The solution to this equation is obtained through an iterative solver, applying the Dirichlet boundary condition at the exhaust gas inlet.

Time-dependent temperatures of both the solid cell and the exhaust gas are determined by employing the Euler-Cauchy method within the MATLAB environment for a time interval of 10^{-3} s. The problem is simplified by making the following assumptions:

- The Converters are placed in a housing, which is designed to offer adiabatic conditions, thereby precluding the possibility of heat loss to the environment.
- The monolith is uniformly considered to be cordierite, with the corresponding material values.
- The air pressure is assumed to be constant at 101,325 Pa.
- The exhaust gas is assumed as ideal gas with a gas constant of R_{sp} = 287 J kg^{-1} K^{-1}.
- It is assumed that the cells are homogeneous, meaning that no temperature gradient is present along the cell surface.
- The reaction processes have no impact on the thermal balance.

Some substance-specific properties of the exhaust gas depend on the current temperature. The following equations (5 to 8) are valid for a pressure below 500,000 Pa and inside a temperature range from 223 K to 773 K [17]. In the context of the interplay among viscosity, heat conductivity, heat capacity, and pressure, it is imperative to acknowledge that the viscosity and heat conductivity of ideal gases can be derived through the framework of kinetic gas theory. Specifically, the mean free path length increases in proportion to the decline in density with decreasing pressure. Consequently, the viscosity and heat conductivity of (not significantly diluted) ideal gases are largely independent of pressure within a considerable range. Additionally, given the relatively low particle densities of ideal gases, it can be postulated that atoms or molecules are not constrained in their molecular motion, thereby ensuring that the heat capacity is largely independent of pressure.

$$\lambda_{gas} = -0.37 \cdot 10^{-3} + 0.103 \cdot 10^{-3} \cdot T_{gas} - 4.657 \cdot 10^{-8} \cdot {T_{gas}}^2 \tag{5 [15]}$$

$$c_{p\,gas} = 1070.3 - 0.564 \cdot T_{gas} + 1.507 \cdot 10^{-3} \cdot {T_{gas}}^2 - 1.102 \cdot 10^{-6} \cdot {T_{gas}}^3 - 1.4 \cdot 10^{-8} \cdot {T_{gas}}^{-2} \tag{6 [15]}$$

$$\eta_{gas} = -3.287 \cdot 10^{-7} + 7.7996 \cdot 10^{-8} \cdot T_{gas} - 4.8801 \cdot 10^{-11} \cdot {T_{gas}}^2 \tag{7 [15]}$$

$$\rho_{gas} = \frac{p}{R_{sp} \cdot T_{gas}} \tag{8}$$

The phenomenon of heat conduction within the catalytic converter, specifically between the cells, is contingent on the temperature differential between the respective cells. The thermal conductivity coefficient assumes primacy in this context, with its value directly influenced by the catalyst material employed. In order to ensure the effective utilization of catalysts, it is imperative to attain the precise light-off temperature and comply with the needed dwell time. Addressing the prevailing issue necessitates the attainment of an ample contact surface between the gas and the heated honeycomb body.

 doi:10.20944/preprints202604.1657.v1

Table 3. Properties of the monoliths for a standardized surface area.

Cell density / cpsi	Wall thickness / mil	A_{int} / m²	Length / in	Length / m	Diamter / m
300	6	7.169	7.113	0.181	0.144
300	8	7.169	7.399	0.188	0.144
400	3	7.169	5.873	0.149	0.144
400	4	7.169	6.000	0.152	0.144
400	6	7.169	6.273	0.159	0.144
600	2	7.169	4.740	0.120	0.144
600	3	7.169	4.865	0.124	0.144
600	4	7.169	4.997	0.127	0.144
750	2	7.169	4.265	0.108	0.144
900	2	7.196	3.915	0.099	0.144
1200	2	7.196	3.424	0.087	0.144

The comparison of different geometries also brings with it the problem of differently sized exchange surfaces. To facilitate a meaningful comparison of the variants, the geometry is dimensioned by measuring the length to an exchange surface of the same size. The ensuing Table provides a comprehensive overview of the salient data pertaining to the diverse geometries in relation to the standardized exchange surface.

Table 4. Weight of the comparative variants.

Weight	300 cpsi	400 cpsi	600 cpsi	750 cpsi	900 cpsi	1200 cpsi
2 mil	-	-	0.392 kg	0.393 kg	0.395 kg	0.397 kg
3 mil	-	0.592 kg	0.596 kg	-	-	-
4 mil	-	0.798 kg	0.806 kg	-	-	-
6 mil	1.214 kg	1.225 kg	-	-	-	-
8 mil	1.653 kg	-	-	-	-	-

It is evident that the substantial variation in catalyst mass has a direct impact on the thermal mass, which in turn exerts a significant influence on the thermal properties (Table). A reduction in thermal mass, while maintaining the same contact surface, results in the potential for more rapid temperature fluctuations. Consequently, the temperature becomes less consistent, thereby increasing the likelihood of the temperature falling below the requisite light-off temperature with greater rapidity.

However, it should be noted that disparities in geometry have the capacity to influence not only the physical properties, but also the process of heat transfer between the gas and the solid. Assuming that the monolith temperature is lower than that of the exhaust gas, this results in a significant heat input, which is determined by the heat transfer coefficient and the surface area of heat exchange. The role of the internal surface, particularly in terms of hosting catalytically active sites, has previously been discussed.

$$\frac{dQ_{conv}}{dt} = \alpha_{gas} \cdot A_{int} \cdot dT \tag{9}$$

The heat transfer coefficient α depend on geometric boundary conditions and fluid properties. In the case of an internally flowed square-channeled geometry, α can be calculated using the Nusselt number (Nu), and the heat conductivity coefficient of the involved gas (λ_{gas}) (Equation 10 and 11) [18].

$$\alpha = \frac{Nu \cdot \lambda_{gas}}{d_{hydr}} \tag{10}$$

 doi:10.20944/preprints202604.1657.v1

Nu is a dimensionless number in heat transfer that represents the ratio of convective to conductive heat transfer across a boundary. It is used to characterize the effectiveness of convective heat transfer in relation to pure conduction. The calculation of the Nusselt number depends on the respective flow case (Equation 11) [16].

$$Nu = \left[3.66^3 + 0.7^3 + \left(1.615 \cdot \left(\frac{Pe \cdot d_{hydr}}{l_{mono}}\right)^{\frac{1}{3}} - 0.7\right)^3\right]^{\frac{1}{3}} \tag{11}$$

The Peclet number (Pe) is a dimensionless number that represents the relative importance of advection (bulk transport) to diffusion (conduction) in heat or mass transfer. It is the product of Reynolds number (Re) and Prandtl Number. In the case of a gas flowing through a honeycomb structure, a high Pe means that convective heat transfer dominates, while a low Pe indicates that heat transfer is mostly through conduction (Equation 12).

$$Pe = Re \cdot Pr \tag{12}$$

The Reynolds number (Equation 13) is a dimensionless number in fluid mechanics and denotes the proportion between the forces of inertia and those of viscosity, which are present in a flowing liquid or gas.

$$Re = \frac{u \cdot \rho_{gas} \cdot d_{hydr}}{\eta_{gas}} \tag{13}$$

The Prandtl number, denoted Pr, is a measure of the interaction between the velocity pattern of a flow field and the temperature field. Pr is typically defined as the ratio of kinematic viscosity to temperature conductivity. By substituting kinematic viscosity with dynamic viscosity and expressing temperature conductivity as the product of heat capacity and heat conductivity of the exhaust gas, Equation 14 is obtained [18].

$$Pr = \frac{\eta_{gas} \cdot c_{p\,gas}}{\lambda_{gas}} \tag{14}$$

Inserting this into the respective equations mentioned above, and including the open area of the substrate A_{open}, finally gives the heat transfer coefficient α for all the monoliths studied (Equation 15) [18].

$$\alpha = \left[49.37 + \left(1.615 \cdot \left(\frac{\dot{m}_{gas} \cdot c_{p\,gas} \cdot {d_{hydr}}^2}{l_{mono} \cdot A_{open} \cdot \lambda_{gas}}\right)^{\frac{1}{3}} - 0{,}7\right)^3\right]^{\frac{1}{3}} \cdot \frac{\lambda_{gas}}{d_{hydr}} \tag{15}$$

Table shows an example of the calculated α values of the analyzed geometries for a mass flow of 100 kg h^{-1} at an exhaust gas temperature of 523 K. This example shows the different orders of magnitude of the variants in relation to each other.

Of particular interest here is the relationship between thermal conductivity and mass. This ratio determines the ability of a honeycomb to change its temperature. As the mass is strongly dependent on the wall thickness, the low wall thickness geometries also have a low mass and therefore a higher heat transfer to mass ratio.

Another parameter of interest in the design and analysis of catalysts for transient applications is the uniformity index (Equation 16). This is a measure of the homogeneity of the temperature distribution over the catalyst. A catalyst with a perfectly uniform temperature will therefore have a value of one, and the greater the inhomogeneity, the smaller the reference value will be.

$$UI = 1 - \frac{\sum_{i=1}^{n} \sqrt{\left(T_{cat\,i} - T_{cat\,avg}\right)^2}}{2 \cdot T_{cat\,avg} \cdot n} \tag{16}$$

 doi:10.20944/preprints202604.1657.v1

The uniformity index is a metric that provides information about the homogeneity of the temperature distribution. The ratio of the active exchange surface to the total available surface is an indicator of whether the required temperature level has been reached. The ratio is derived by dividing the contact area that has attained the requisite light-off temperature by the total available area (Equation 17). This value, therefore, provides insight into the active catalyst area. A larger value indicates a greater area that is currently in use.

$$A_{Ratio\ Activ} = \frac{A_{light-off}}{A_{int}} \tag{17}$$

Table 5. Matrix for the heat transfer value of the selected monoliths.

α-value / W m^{-1} K^{-1}	300 cpsi	400 cpsi	600 cpsi	750 cpsi	900 cpsi	1200 cpsi
2 mil	-	-	151.8	170.7	188.0	219.2
3 mil	-	125.4	155.8	-	-	-
4 mil	-	128.1	160.0	-	-	-
6 mil	114.0	134.0	-	-	-	-
8 mil	118.5	-	-	-	-	-

5. Discussion of Results

In the field of automobile manufacturing, the utilisation of honeycomb body geometries as a foundation for the integration of catalytic converters has become a predominant practice. A geometry that is employed with great frequency is the monolith with 400 cpsi [19]. In this study the geometry with 400 cpsi and 4 mil is consider as refence for comparison. The selection of geometry is contingent on various factors. The contact area between the raw gas and the catalyst surface is pivotal for the catalytic reaction. It is imperative that there is sufficient surface area for the reaction to occur, and that the defined light-off temperature is attained. This necessitates a rapid attainment of the required temperature in the cold state, for which the mass is a contributing factor. Concurrently, both thermal and kinetic loads must be considered. The thermal stress can be attributed to the maximum exhaust gas temperature, which is significantly higher for petrol engines than for diesel engines, and the thermal shock during cold start. The ambient temperature and the load profile play a particular role here. The kinematic stresses can be categorised into two distinct types: the vehicle's inherent vibrations, such as those induced by the engine, and the dynamic driving stresses. Specifically, accelerations resulting from impacts, such as potholes or uneven road surfaces, are significant contributors to these stresses. Additionally, the pure driving dynamic loads, due to accelerations in all axes, play a substantial role.

The calculation was applied to the recorded driving cycle. First, the cold start cycle without the start-stop system was considered Figure . The following figures compare the same cell densities. It should be noted that the catalyst geometries have been adjusted for length so that the same contact area between the gas and the honeycomb body is available for all variants. The reference model of 7.169 m² was used as the basis. For a direct comparison between the various geometries examined within a given scenario, please take note of the appendix, which contains a set of comparative diagrams.

5.1. Cold-Start w/o Start-Stop System

As illustrated in the diagram, the ordinate denotes the temperature, with the exhaust gas temperature prior to the catalytic converter and the average temperature curves of the respective geometries. The abscissa indicates the ratio of the contact area over light-off temperature to the total contact area. The values are plotted over time on the x-axis.

As demonstrated in Figure , the impact of varying wall thicknesses on the system's thermal performance is shown. It is evident that the thinnest wall thickness demonstrates a faster response to

 doi:10.20944/preprints202604.1657.v1

temperature fluctuations, resulting in accelerated heating in the starting phase of the cycle. It is noteworthy that, in the initial phase, the ratio of the active area for 3 mil material thickness surpasses those of the other two variants. However, in the subsequent phase, the variant with the thickest wall demonstrates remarkable consistency, maintaining an average temperature. This analysis indicates that the 3 mil variant is the best choice of this three for the initial phase of the cold boot.

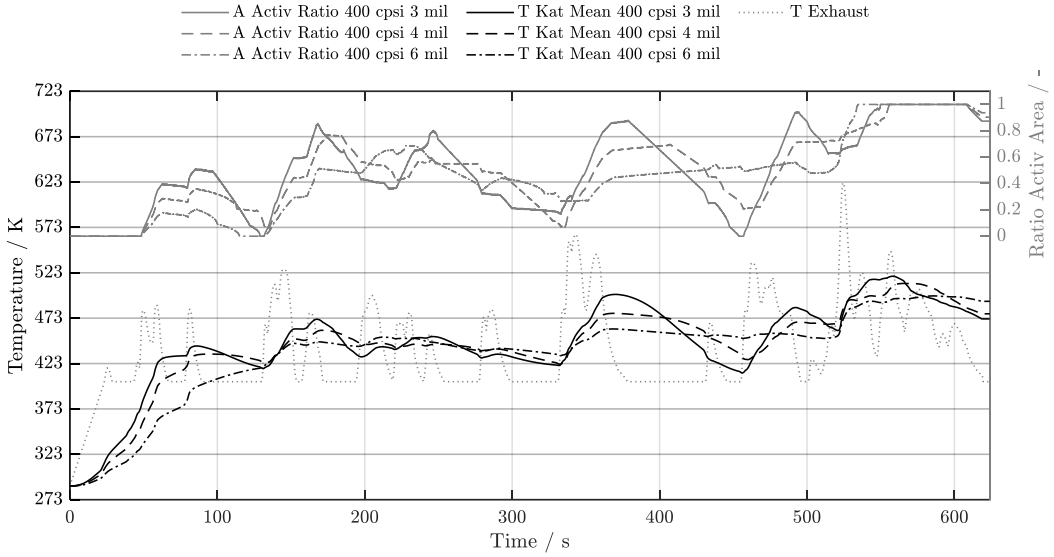

Figure 6. Temperature trend of the 400 cpsi series during cold start w/o start-stop system.

A notable observation is that, particularly in the second half of the test, this category consistently exceeds the requisite temperature. When the entire test duration is taken into account, this proportion increases to 58.0 %, which is the highest percentage above the light-off level (3 mil = 50.7 %, 4 mil = 52.7 %). The influence of the thermal mass is evident in these three variants. While rapid heating is advantageous at the beginning and thus the lighter variants have an advantage, maintaining the temperature becomes increasingly important during the course of the test, in which the more massive geometries then have an advantage.

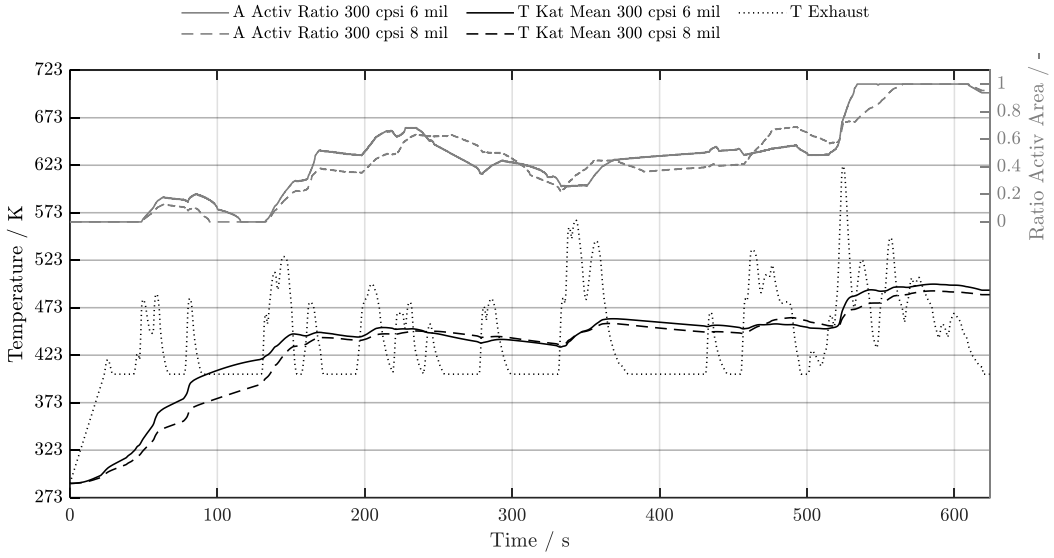

Figure 7. Temperature trend of the 300 cpsi series during cold start w/o start-stop system.

The variants with reduced cell density of 300 cpsi (Figure) have a much higher mass, as a significantly larger honeycomb body is required to achieve the same exchange surface area. This previously observed trend persists. In contrast, it was observed that higher cell densities resulted in

 doi:10.20944/preprints202604.1657.v1

a more pronounced buffering effect. This suggests that the maximum deflections are dampened and the average temperature remains relatively constant. The curves of both variants demonstrate significant similarity, with the most notable disparity occurring at the initial stages. During the middle phases, which include instances of standstill events, both variants exhibit a strong parallelism with each other.

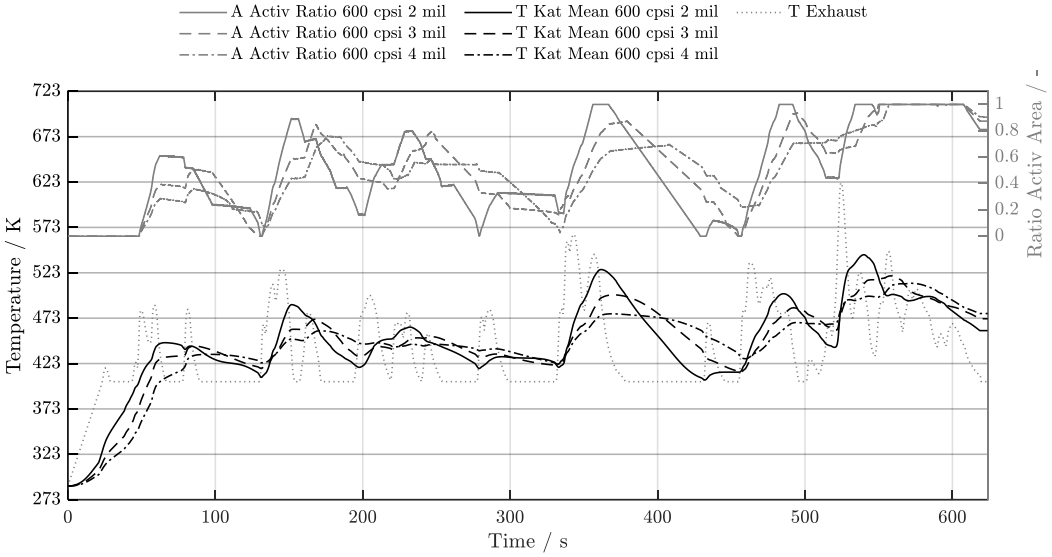

Figure 8. Temperature trend of the 600 cpsi series during cold start w/o start-stop system.

However, a notable disparity emerges in the duration required to attain the initial light-off temperature. Specifically, the 6 mil version reached this threshold after 54 s, while the heavier version required a substantially longer 207 s. When the entire duration over light-off is considered, the 6 mil variant attains the maximum value among the tested variants for this scenario, reaching 58.2 % of the test duration (8 mil = 55.4 %).

Notably, the heaviest of the 400 cpsi variants still achieved the best value in this category, but in this scenario, it was the lighter variant that emerged as the optimal choice. This outcome indicates the presence of an optimal weight value for this particular test scenario, and it suggests that the 300 cpsi with 8 mil variant has already surpassed this threshold. Consequently, the additional weight imposes a detrimental effect, as insufficient thermal power is transferred from the exhaust gas to the body to elevate the energy level sufficiently.

The results of the 600 cpsi series (Figure) show a significantly faster heating process compared to the results previously considered. After just 60 s, the test specimen with 2 mils exceeds the ratio of 0.5 of the exchange surface over light-off temperature in ratio to the total contact surface for the first time. Furthermore, complete heating of the monolith above light-off temperature is also achieved several times.

The influence of the wall thickness is evident in the figure through the varying gradients, with thinner walls demonstrating faster temperature adaptation. This phenomenon can be attributed to the disparate thermal mass. As illustrated in Table , the 4 mil body exhibits a weight that is nearly double that of the 2 mil variant. When the range between seconds 320 s and 500 s is considered, the increase in the smallest wall thickness is particularly pronounced in comparison to the other two. The body's heating up to its light-off temperature and subsequent cooling rate were found to be contingent upon the thickness of the wall, with thicker bodies requiring more time to cool down. It is noteworthy that the reference value of 0.5 for the ratio of active area is maintained for a substantially longer duration in the 4 and 3 mil variants when compared to the 2 mil configuration, owing to the former's higher heat capacity and slower cooling rate. This is also reflected in the achievement of the light-off temperature. While the 2 mil version reaches the required level in only

 doi:10.20944/preprints202604.1657.v1

49.4 % of the test time, the other two reach it in more than half the time (3 mil = 50.8 % and 4 mil = 52.6 %).

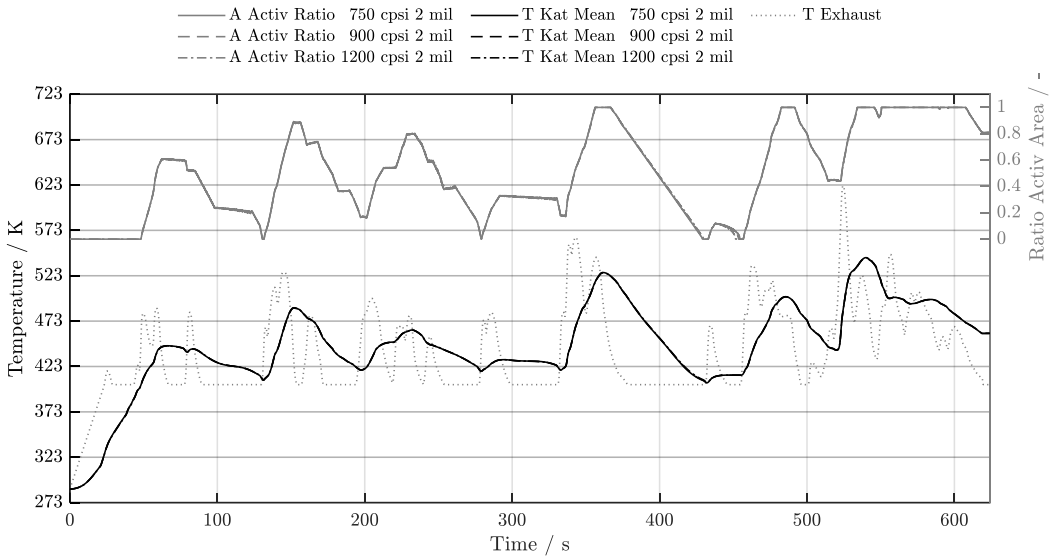

Figure 9. Temperature trend of the high cell series during cold start w/o start-stop system.

The final comparison in this section focuses on the so-called high cell types, which are characterized by a uniform wall thickness of 2 mils across all variants. These designs exhibit a high degree of sensitivity to changes in conditions, as illustrated by the diagram, which reveals minimal differences among them. The trend (Figure) in these variants is nearly linear, with only slight deviations in some areas. A detailed examination of Table reveals that the key parameters for these variants are highly comparable. The disparity in weight between the heaviest (1200 cpsi) and lightest (750 cpsi) bodies is minimal, amounting to only $4 \cdot 10^{-4}$ kg. Given the equalization of the contact area between the gas and the catalytic surface, and the negligible difference in weight, it can be concluded that the curves are equivalent. When the curve for the 600 cpsi body with a 2-mil wall thickness is also considered, it becomes evident that this exhibits a nearly identical curve and a mere 0.3% disparity in weight compared to the 750 cpsi variant. However, a significant discrepancy in length emerges, with a nearly 30 % variation. It can be concluded that as cell density increases, the catalyst utilized can be reduced in size while maintaining the same catalytic area, thereby optimizing the design. Despite the fact that the light-off temperature is attained after a time of only 27.8 s, the values over the cycle are rather low. It is noteworthy that a body made of 2 mil reaches an average temperature above the light-off temperature in only 49.4 % of the cycle time. This outcome is the lowest observed in this particular scenario. The simulation dataset for this particular setting can be found in full in Appendix A1, with an overview of all the data presented in the form of charts. This allows for more straightforward direct comparison.

5.2. Cold-Start w/ Start-Stop System

The integration of start-stop systems in contemporary vehicles signifies a pivotal innovation aimed at curtailing fuel consumption and minimizing CO_2 emissions. This technology automatically deactivates the engine when the vehicle is stationary, such as during traffic signals or in congested traffic, and seamlessly reactivates it when the driver accelerates or releases the brake. In urban driving conditions, where frequent stops and starts are prevalent, start-stop systems can result in fuel savings of up to 10 % dependent on the drive profile , thereby markedly enhancing vehicle efficiency [19]. Moreover, these systems contribute to the reduction of greenhouse gas emissions, thereby assisting automakers in complying with increasingly stringent environmental regulations, such as the Euro VII emission standards that impose strict limits on pollutant output. Beyond regulatory advantages, start-stop systems also enhance sustainability by decreasing air pollution, particularly in densely

 doi:10.20944/preprints202604.1657.v1

populated urban areas where vehicle emissions contribute to lower air quality. In addition, in modern-day vehicles—particularly those equipped with mild hybrid technology—start-stop systems collaborate with regenerative braking and advanced energy management systems to enhance performance while preserving driving comfort. Through the integration of these technologies, manufacturers not only enhance fuel efficiency but also contribute to the global efforts toward a more environmentally friendly and sustainable transportation sector.

The ensuing figures illustrate the outcomes of the calculations with the start-stop system enabled for this particular urban driving cycle. The salient distinction in this case is that no exhaust gas enters the catalytic converter when the engine is deactivated, thereby ensuring that the catalytic converter's temperature remains constant during the vehicle's idling period with only heat transport effects inside the catalytic converter, whereby temperature gradients along the honeycomb getting balanced.

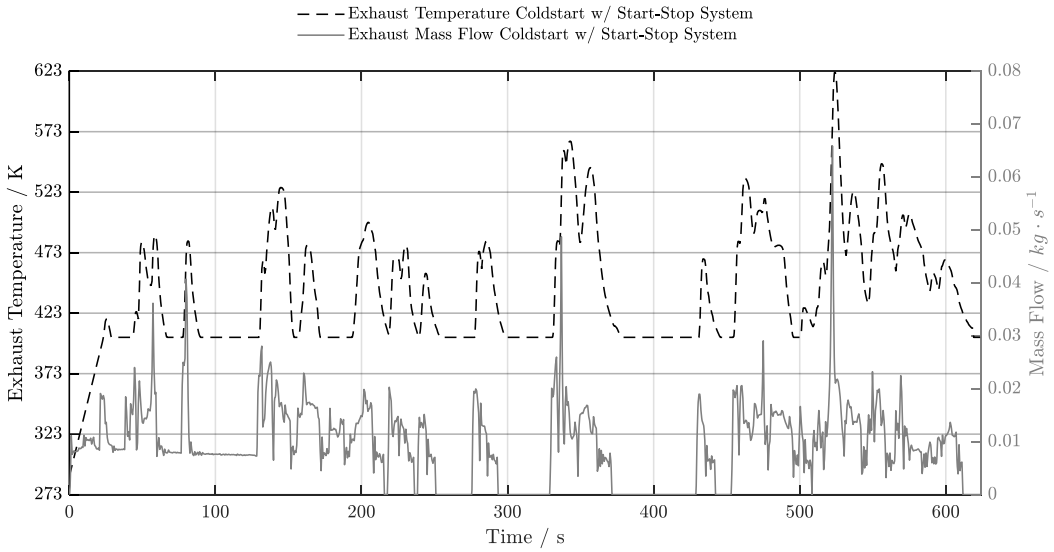

Figure 10. Exhaust gas temperature curve and exhaust gas mass flow curve for cold start w/ start-stop system.

Figure demonstrates the exhaust gas flow for the cold start scenario with activated start-stop system. The engine warm-up strategy serves to prevent the engine from being switched off if the engine temperature is too cold or the system voltage is too low. It is noteworthy that the system's initial activation occurs after an operational duration exceeding 200 s, thereby ensuring that any observed variations in outcomes manifest only from this subsequent point onwards.

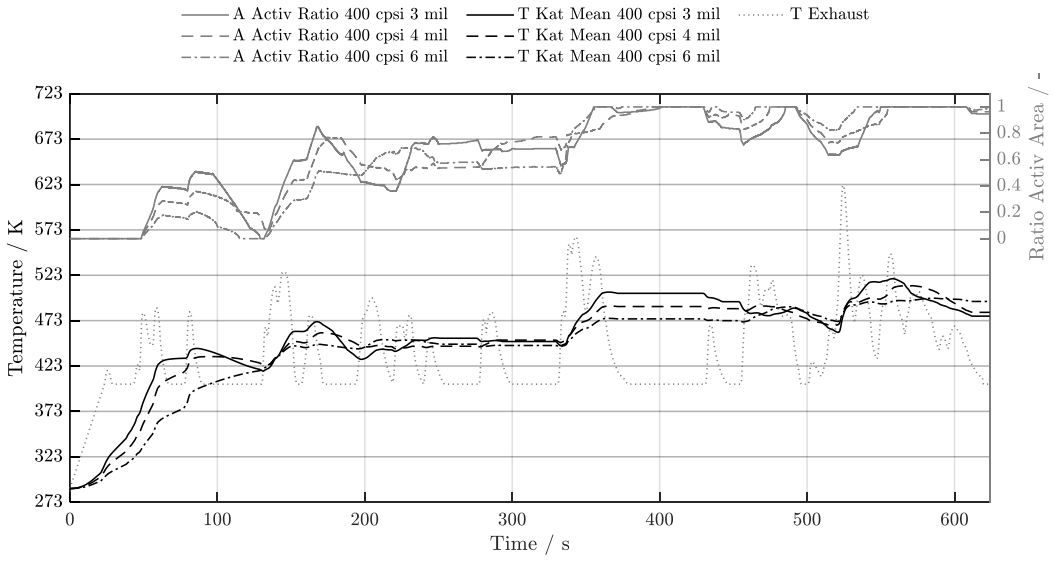

Figure 11. Temperature trend of the 400 cpsi series during cold start w/ start-stop system.

 doi:10.20944/preprints202604.1657.v1

The outcomes of the 400 cpsi series (Figure) demonstrate a notable distinction when compared with results obtained without the start-stop system. An examination of the active exchange surface is of particular interest. It is evident that this value is significantly higher for all three bodies with a start-stop system, reaching a complete heating of the honeycomb above light-off level on multiple occasions in the latter half of the cycle. In the phase between 200 s and 330 s, the temperature lines in this diagram exhibit a marked horizontal tendency, contrasting with the preceding linear downward trend.

The start-stop system's impact is multifaceted. Primarily, it prevents the release of emissions into the environment during engine standstill. Secondly, it hinders the cooling process, ensuring that the catalytic converter surface heats up more rapidly and attains the required temperature more quickly. Additionally, elevated temperatures are attained, as evidenced in Figure , enhancing the catalytic converter's conversion rates and further reducing emissions.

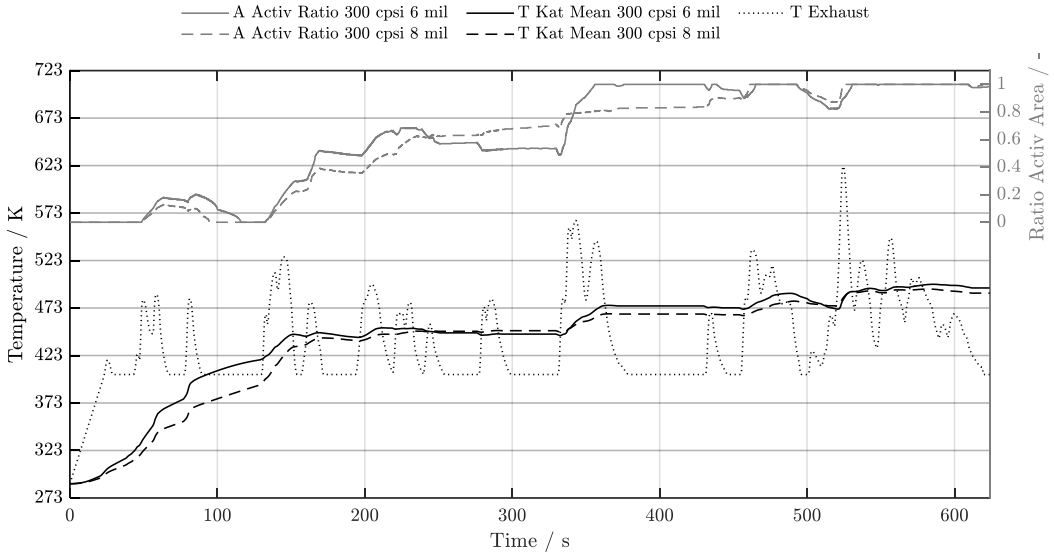

Figure 12. Temperature trend of the 300 CPSI series during cold start w/ start-stop system.

A comparison of the trend curves for these two variants in Figure reveals that they are significantly flatter than those of the other types. Furthermore, when the engine is switched off at standstill, the trend curve becomes even flatter. At the initiation stage, a discernible disparity in wall thickness persists between the two variants. The thinner version attains the initial light-off level after 149 s, while the heavier version requires 207 s. While the proportion of time within which the light-off temperature is reached increases significantly for both bodies, the 6 mil version still has an advantage (6 mil = 72.4 %, 8 mil = 66.8 %). The ratio of the active to the total contact area indicates that the 6 mil version attains complete heating much earlier. This suggests that the complete surface is available for catalytic conversion.

In an earlier work [9] a difference of 30 % in the heat-up time for these two variants were calculated, which roughly corresponds to the difference in weight. The load cycle without engine shutdown at standstill also demonstrates this difference during initial heating. However, the difference decreases significantly after both variants have reached a certain temperature level (400 K). The disparity in mass-related rates of temperature change is counterbalanced, resulting in a net effect that is nearly imperceptible. However, a modest advantage is observed for the 6 mil variant across the range of investigated temperatures. The application of start-stop technology reveals that, while the thinner variant initially exhibits higher temperatures, it cannot maintain this advantage over the entire range. In the middle section, the temperature of the variant with a larger cell wall is even higher in certain phases. However, in the middle and final phases, the temperatures of both variants become almost equal. In summary, the 6 mil variant has advantages in reaching and maintaining the light-off temperature and also in the ratio of the active to the total contact area.

 doi:10.20944/preprints202604.1657.v1

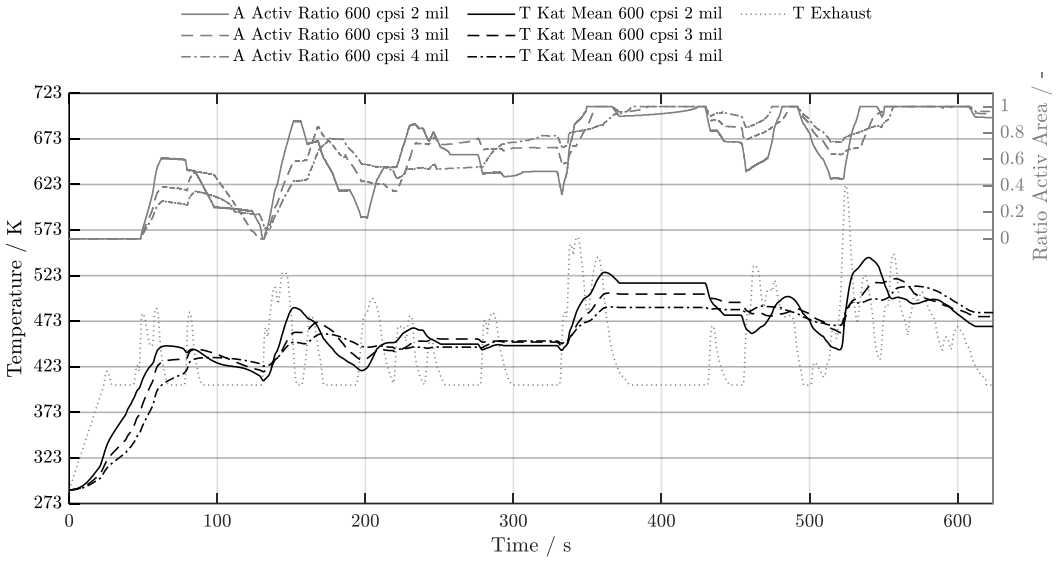

Figure 13. Temperature trend of the 600 cpsi series during cold start w/ start-stop system.

The trend of all three 600 cpsi variants (Figure) is significantly less fluctuating with the start-stop system activated than in its deactivated state. Conversely, the temperature levels exhibited by all variants are considerably elevated. For the 600 cpsi models, the difference with or without engine shutdown is very clear. It is noteworthy that values exceeding 70 % can be attained with the system, with 2 mil achieving 71.9 %, 3 mil reaching 70.4 %, and 4 mil achieving 73.6 %. Therefore, the improvement is approximately 20 % in relation to the operating time. However, it should be noted that the start-stop system only takes effect after approximately 200 s.

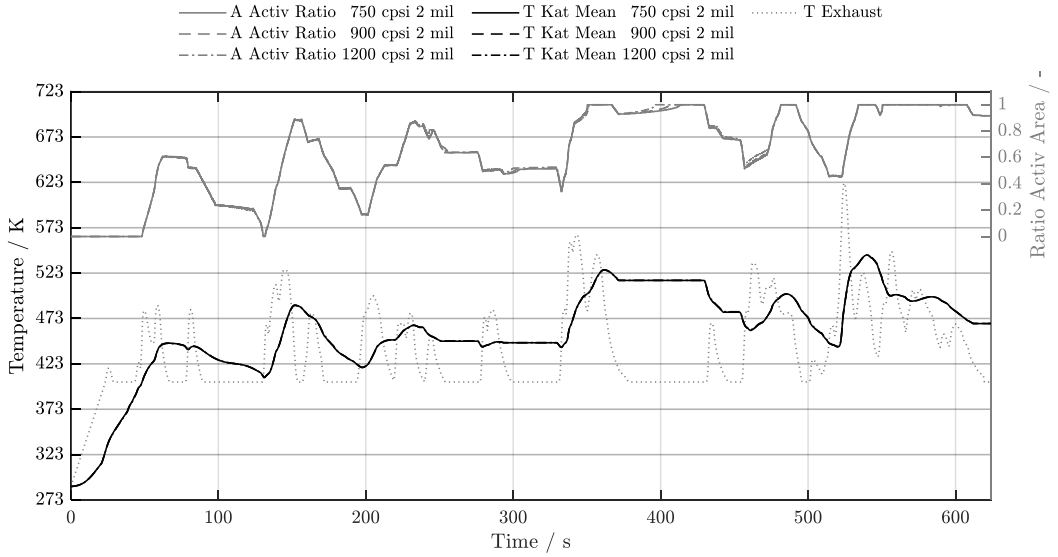

Figure 14. Temperature trend of the high cell series during cold start w/ start-stop system.

The variants exhibiting a high cell density in Figure demonstrating a high degree of similarity with regard to the temperature curve. While the disparities are more pronounced than in the preceding experiment, the similarity remains marked. All three tested items demonstrate a highly comparable trend, with no significant disparities observed. Despite the heightened visibility of the differences in this instance, they remain negligible. It is noteworthy that the trend observed in the 600 cpsi and 2 mil variant can also be incorporated and is found to be almost identical. For all bodies with this thin wall thickness, the difference between with and without motor shutdown is the most pronounced. It can thus be concluded that the variants with low cell density, especially in combination with a start stop system, are best suited to achieving high conversion rates. The

 doi:10.20944/preprints202604.1657.v1

simulation dataset for this particular scenario can be found in full in Appendix A2, with an overview of all the data presented in the form of charts. This allows for more straightforward direct comparison.

5.3. Warm-Start w/o Start-Stop System

In this section, the temperature profile for an urban driving cycle is considered, where the system has already been warmed up. To this end, the cycle that would have been initiated with a cold start is once again run through. The objective is to demonstrate that, upon completion of the journey, the vehicle comes to a halt, the engine is deactivated, and then subsequently reactivated. This results in a significantly more pronounced increase in exhaust gas temperature at the start-up, as the system is already preheated and the exhaust gas enters the catalytic converter at a higher temperature (Figure).

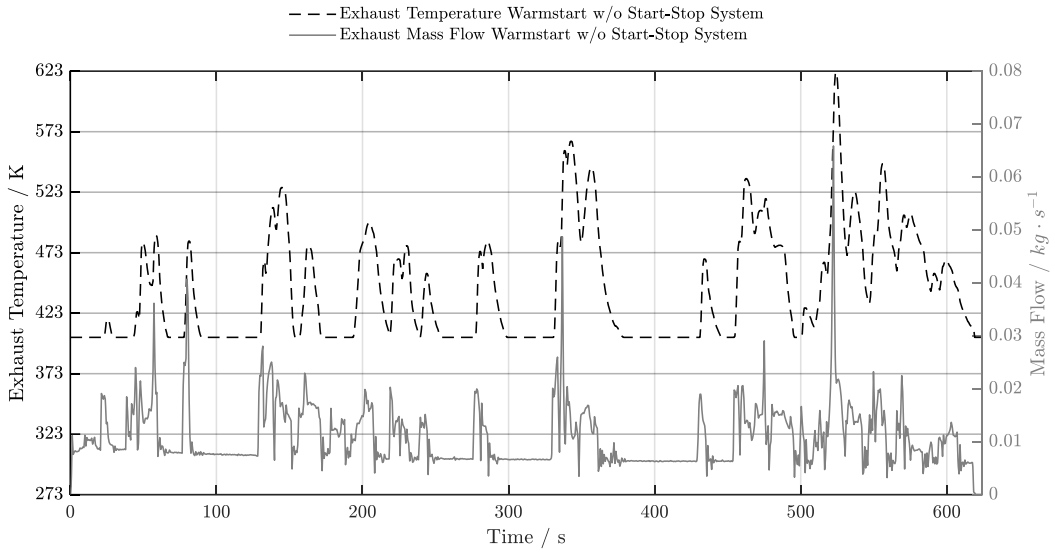

Figure 15. Exhaust gas temperature curve and exhaust gas mass flow curve for warm start w/o start-stop system.

Consequently, the starting condition for each test type is contingent on its behavior in the cold start cycle. The objective is to replicate the actual starting conditions with the greatest possible accuracy.

The results plot for the 400 cpsi series (Figure) demonstrates the discrepancy between the two cycles immediately at the inception of the process. It is evident that all three variants initiate at a level that is considerably higher than that of the exhaust gas. The rapid thermal response of the lightest variant results in a sharp temperature drop at the onset. The analysis indicates that the pre-tempered state attains equilibrium following a brief cycle duration, with the temperature curve demonstrating a progressive convergence towards that of the cold start. For the two heavier variants, the effect of preheating lasts longer, but there is also no striking advantage. It is notable that in the latter stages of the test, there is no discernible visual distinction between the cold and hot start.

 doi:10.20944/preprints202604.1657.v1

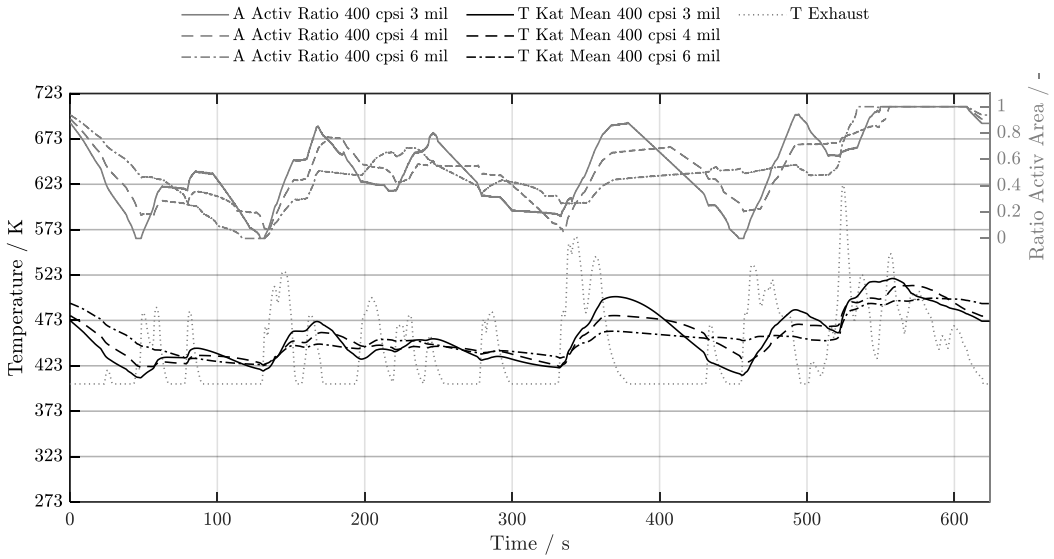

Figure 16. Temperature trend of the 400 cpsi series during warm start w/o start-stop system.

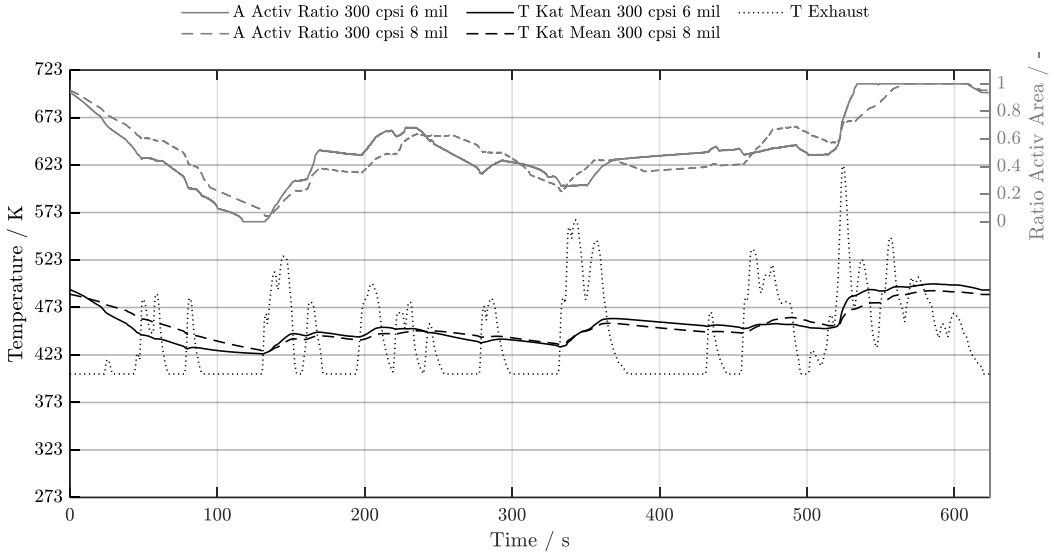

Figure 17. Temperature trend of the 300 cpsi series during warm start w/o start-stop system.

The 300 cpsi series has the highest mass, which means that these variants also have the most constant temperature curves. Due to their comparatively high thermal storage capacity, these two variants should also be able to retain an advantage for as long as possible in the pre-tempered start scenario. However, it should be noted that even these variants demonstrate in Figure that the advantage is negated by downtimes and the consequent low exhaust gas temperature, after a short period of driving. This finding underscores the paramount importance of not only attaining the requisite temperature but also sustaining it, a consideration that is particularly significant in urban driving.

The available data indicates that the system should be subdivided. The system should comprise a short catalytic converter with a high cell density and low wall thickness upstream, facilitating rapid temperature adjustments during the heating process, and a larger converter with a lower cell density and higher wall thickness downstream, compensating for brief periods when the vehicle is stationary.

The monolith with 300 cpsi and 8 mil demonstrates the most significant effect between cold and warm start scenarios for the duration over light-off of all the variants examined. For this scenario the 6 mil type achieves 66.1 % and the 8 mil type 68.4 %. It is worth pointing out that the second part of the driving profile bears a close resemblance to the cold start scenario. The simulation dataset for this

 doi:10.20944/preprints202604.1657.v1

particular scenario can be found in full in Appendix A3, with an overview of all the data presented in the form of charts. This approach facilitates a more straightforward direct comparison.

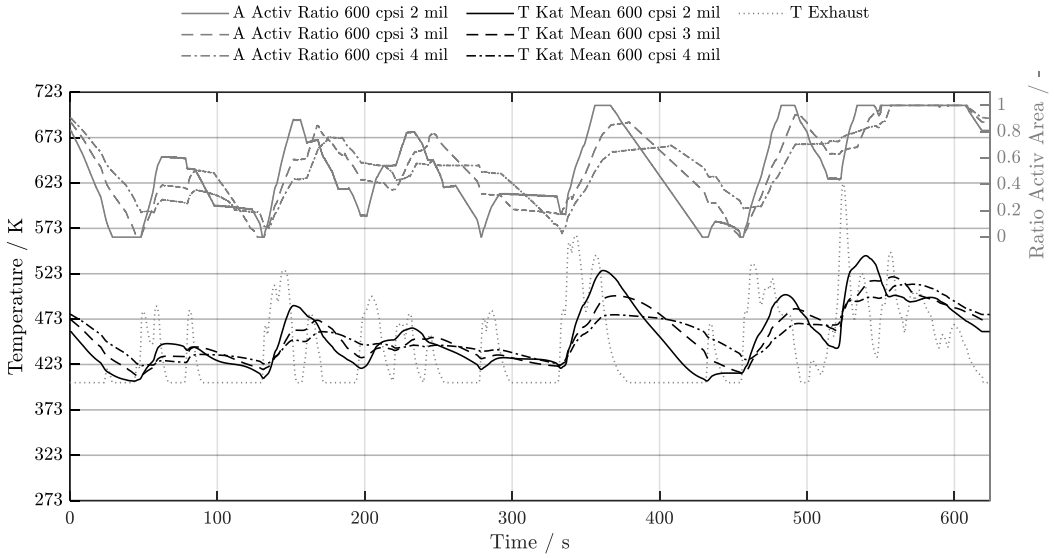

Figure 18. Temperature trend of the 600 cpsi series during warm start w/o start-stop system.

The 600 cpsi geometries have a high temperature change capability. As a result, the temperatures here adapt quickly to changes in exhaust gas temperature, and the difference between cold and warm starts for all three variants is equalized after the first extended standstill of the vehicle (approx. 120 s in Figure). It is noteworthy that, in terms of time over light-off, the honeycomb body with a 4 mil wall thickness achieved the highest result of the 600 cpsi series at 87.2 %, and the improvement between hot and cold starts was still the greatest here.

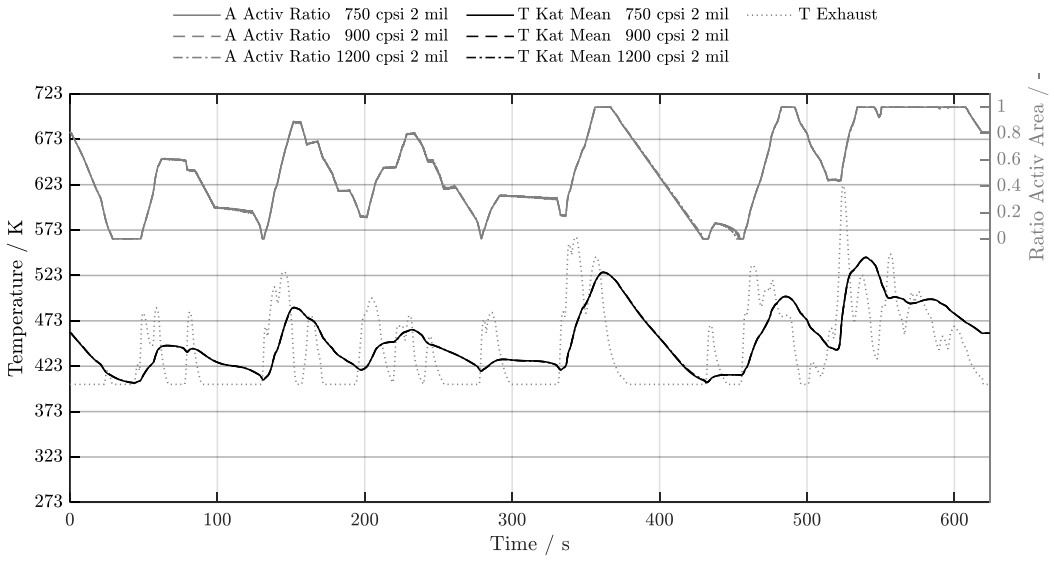

Figure 19. Temperature trend of the high cell series during warm start w/o start-stop system.

Even faster than the 600 cpsi variants, those with even higher cell densities can respond to temperature jumps which are shown in Figure . As a result, the differences here (including the 600 cpsi and 2 mil) are the smallest. Once again, running the engine when the car is stationary has a more negative effect on the temperature of these models than it does on models with a higher thermal capacity.

 doi:10.20944/preprints202604.1657.v1

5.4. Warm-Start w/ Start-Stop System

The preceding results indicated that deactivating the engine when the vehicle is not in motion has a significant effect on catalyst temperatures.

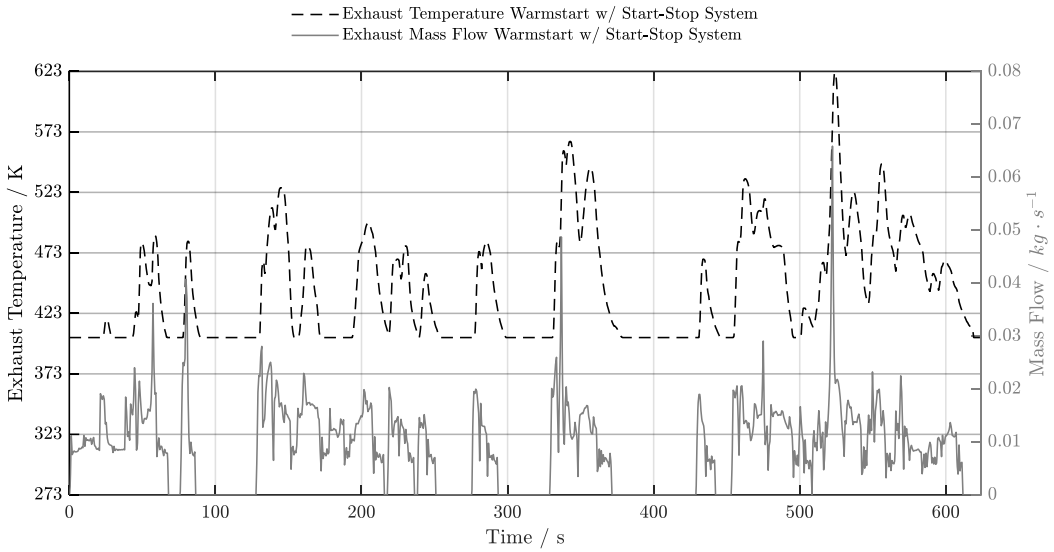

Figure 20. Exhaust gas temperature curve and exhaust gas mass flow curve for warm start w/ start-stop system.

The subsequent results demonstrate a highly plausible scenario, wherein the system is already pre-heated due to urban driving conditions and persists in operating within metropolitan areas. The therefore used exhaust temperature and mass flow trend is illustrated in Figure . A case study of Germany lends further credence to this scenario. There, it is estimated that approximately 65 % of the working individuals commute to their places of employment by automobile on a daily basis [20]. The majority of these drive into urban areas. This suggests that a typical urban driving profile characterized by low speeds, low load requirements and frequent standstill phases at traffic lights, junctions or convoy traffic is run through after the system has been preheated.

In the initial phase of the cycle, the preheating procedure exerts a discernibly beneficial effect on the temperature levels of all three curves in Figure . The engine deactivation during the initial extended interval (by approximately 100 s) exerts a highly favorable effect in this instance. Utilizing the model with 400 cpsi and 3 mil as a case study for comparison across the four scenarios, the results are particularly evident.

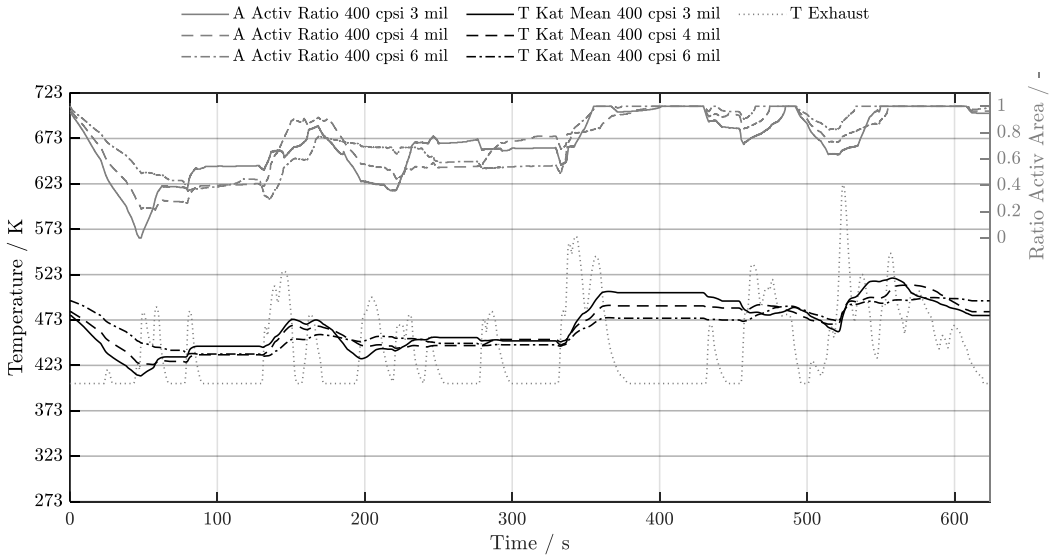

 doi:10.20944/preprints202604.1657.v1

Figure 21. Temperature trend of the 400 cpsi series during warm start w/ start-stop system.

A noteworthy finding emerges when considering only the period within the cycle during which the average catalytic converter temperature reaches or exceeds the light-off temperature. In the absence of the start-stop option, the values recorded were 50.7 % and 53.8 % for the cold and warm starts, respectively. Conversely, the values with engine shutdown are significantly higher at 70.4 % (cold engine start) and 75.9 % (hot engine start). This finding indicates that the impact of the start-stop system is considerably more pronounced than that of preconditioning. It is important to note that these values are based on the entire duration of the test and not just that with the engine running.

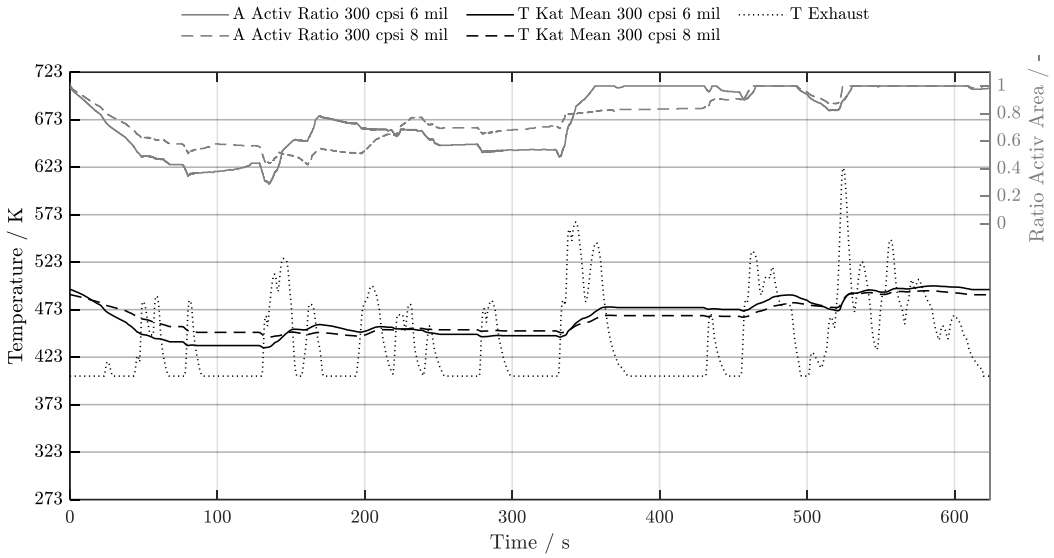

Figure 22. Temperature trend of the 300 cpsi series during warm start w/ start-stop system.

The result for the active contact area is evidently the highest in this instance (Figure). In the second half, the values for both variants, with only short intermediate phases, demonstrate that the entire catalytic converter attains the light-off temperature, thereby facilitating optimal conversion rates. It is noteworthy that this outcome was also attained during the second half of the test when the cold start was executed with the start-stop system activated. However, the initial phase exhibits a substantially higher level in comparison to all other honeycomb bodies. Nevertheless, it is evident that the performance of the two 300 cpsi variants differs from each other, particularly in the initial section. The 8 mil version is the heaviest and therefore also the most thermally inert body. This configuration also enables the optimization of the effect of preheating, particularly in conjunction with the start-stop system. In this scenario, the 300 cpsi and 8 mil variant is the only one to achieve the phenomenon of remaining above the light-off level at all times across all tests.

This candidate exhibits the most negligible fluctuations, consequently yielding a remarkably flat curve. When the minimum and maximum temperatures are also taken into account, it becomes evident that a fluctuation of only 48.6 K occurs in this instance. It is noteworthy that if a specific temperature is attained, it can be maintained with exceptional consistency. However, if this is below the required temperature, it is also very difficult to increase it. This configuration is therefore advantageous when pre-tempered and further protected from cooling through the utilization of an automatic start-stop function. It is also important to consider how much power can be transferred to the monolith with the help of the exhaust gas. It is noteworthy that engines operating under low loads may encounter difficulties in attaining the requisite temperature levels if such geometries are employed.

 doi:10.20944/preprints202604.1657.v1

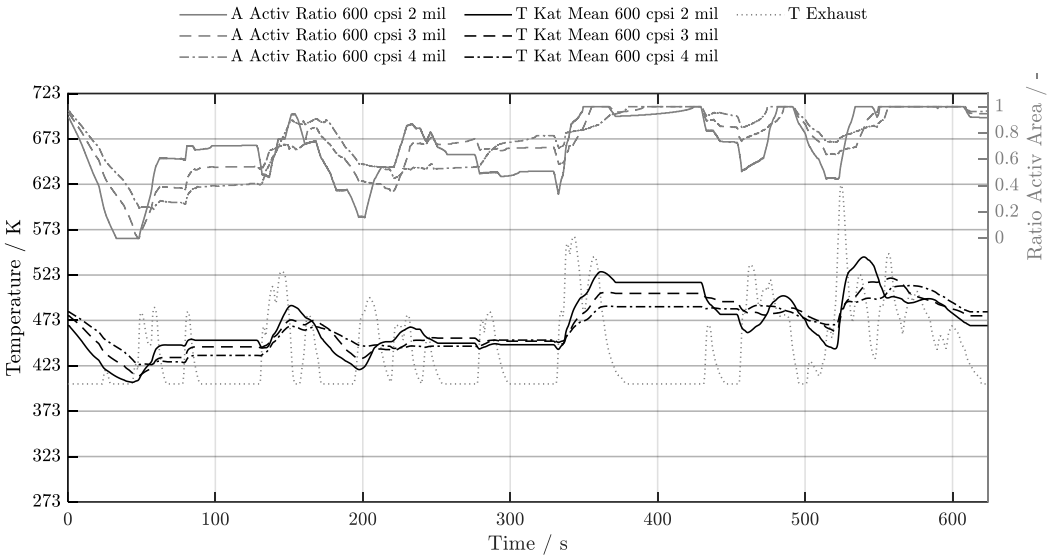

Figure 23. Temperature trend of the 600 cpsi series during warm start w/ start-stop system.

The 2 mil variant of the 600 cpsi series is of particular interest, as it exhibits results that closely resemble those of the high-cell variants. The plot in Figure provides a comprehensive summary of the tested variants. The rapid response of the thinnest version is unable to sustain the benefit of the preheated state for an extended period. Consequently, the monolith cools down prior to the initial extended period of inactivity at light-off temperature. The remaining versions are in a position to benefit from this phenomenon for a significantly extended period. Despite the heaviest version in this series exhibiting a lower average temperature and only attaining complete heating above light-off level for brief intervals, it does not sink to a considerable extent, with at least 20 % of the contact surface consistently remaining active. This analysis underscores the fact that each variant possesses distinct advantages and disadvantages within specific parameters.

In accordance with the findings of preceding investigations, this aligns coherently with the overarching data. The high-cell variants, characterized by their minimal mass, exhibit the most pronounced sensitivity to temperature fluctuations and consequently demonstrate a remarkable capacity for rapid adaptation.

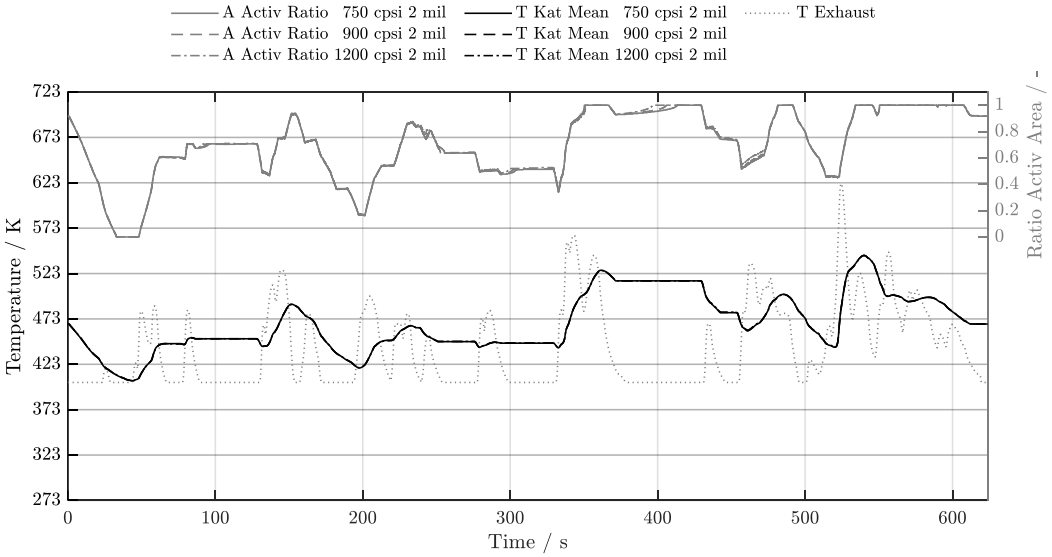

Figure 24. Temperature trend of the high cell series during warm start w/ start-stop system.

Consequently, the benefits of conditioning are only sustained for a brief duration in Figure , and once more, all processes, inclusive of the 2 mil with 600 cpsi variant, manifest near-identical

 doi:10.20944/preprints202604.1657.v1

characteristics. The light-off temperature is achieved in just under 84 % of the test time (750 cpsi = 83.8 %, 900 cpsi = 83.9 %, 1200 cpsi = 84.0 %), indicating that the peak value of the 300 cpsi with 8 mil variant cannot be attained, though it remains at a high level. The simulation dataset for this particular scenario can be found in full in Appendix A4, with an overview of all the data presented in the form of charts. This allows for more straightforward direct comparison.

5.5. Electrical Preheating

In the context of ascending emissions regulations on a global scale, there has been a discernible trend towards the implementation of increasingly sophisticated exhaust gas aftertreatment systems. Concurrently, the utilization of electric catalytic converter preheating is gaining popularity. High-performance car manufacturer are increasingly relying on this technic for their hyperarcs. Nevertheless, as the requirements escalate, the probability of its implementation in series production models concomitantly rises.

The objective of this innovation is to automatically preheat the catalytic converters prior to engine ignition, thereby ensuring that they attain a light-off temperature at the start of operation. The implementation of such automated starting sequences can be facilitated by diverse systems. Hybrid vehicles offer distinct advantages in this regard. Firstly, the battery capacity and maximum amperage of this category are substantial, making it highly conducive to electric heating. Additionally, the exhaust gas aftertreatment system in these vehicles can be heated while the vehicle is initially driven purely electrically. In the case of vehicles devoid of the option of electric propulsion, techniques such as the keyless system can be employed, which recognizes when the vehicle key is in the immediate vicinity and can activate the pre-heater from this point onwards.

A variety of techniques and options exist for the heating of the catalytic converter. A number of these techniques have already been commercialized, while others are still undergoing experimental phase. The product range includes heated sections and fully heated metal carriers. Concurrently, electrically heatable ceramics have emerged as a potential alternative carrier material, superseding cordierite [12]. Such a hybrid ceramic has properties analogous to cordierite, yet it is electrically conductive, enabling direct energization and utilization as an ohmic heating resistor. The resistance across the catalytic converter is approximately 1 Ω. When employed in conjunction with the 48-volt electrical systems prevalent in contemporary vehicles, this configuration can generate a heating output of 2.3 kW. The material specific parameters for the simulation model are listed in Table .

Table 6. Overview of the most important material parameters for cordierite and hybrid ceramic.

Material	Cordierit	Hybrid Ceramic
Density ρ	2100 kg m^{-3}	2670 kg m^{-3}
Heat Capacity c_p	1000 J kg^{-1} K^{-1}	805 J kg^{-1} K^{-1}
Thermal Conductivity λ	2.0 W m^{-1} K^{-1}	4.7 W m^{-1} K^{-1}

The implementation of such a system can be achieved through a variety of methodologies. Firstly, it is necessary to determine whether only the upstream part of the catalytic converter should be heated or whether the entire body should be constructed from electrically conductive material. Additionally, a decision must be made regarding the strategy for determining when the heating process should commence. The most evident strategy would be to initiate the process prior to engine ignition, thereby rendering the initial emissions of the combustion process innocuous. However, extant findings demonstrate that pure preheating of the system exerts only a transient effect on the thermal household, contingent on the geometry of the catalytic converter employed. Consequently, the standstill phases of the vehicle could be utilized to repeatedly augment the temperature as required. However, this approach is disadvantageous due to the fact that during these periods, the entire electrical vehicle supply is derived from an on-board battery, which consequently experiences an augmented load. Consequently, from the perspective of energy balance, it is more rational and feasible to implement activation of the heating during engine operation.

 doi:10.20944/preprints202604.1657.v1

The implementation in the simulation model is carried out using an additional energy term. The adapted initial situation is illustrated in the following figure. As illustrated in the above Figure , the model has been expanded to include supplementary electrical heating energy.

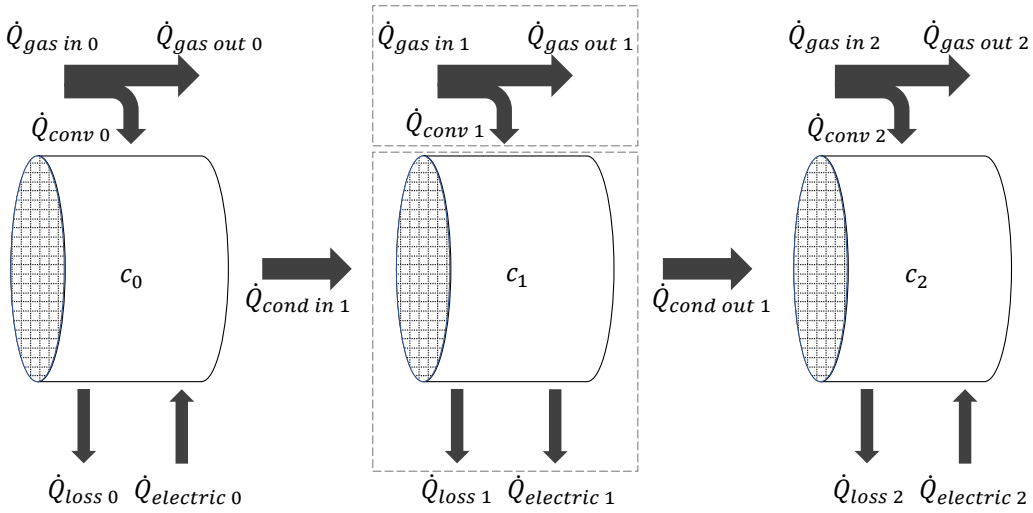

Figure 25. Illustration of the cell modelling of the calculation system including the electrical heating energy.

This additional option consequently engenders a substantial number of potential implementation variants. For instance, the electrical preheating of the system for 30 s prior to the start-up of the engine is shown in this work. It is important to note that the time scale in Figure now starts at minus thirty seconds, so that this additional preheat time can be included without having to change the rest of the cycle. In addition to the reference dimension, the heaviest variant (300 cpsi with 8 mil) and a high-cell model (900 cpsi with 2 mil) are simulated for comparison.

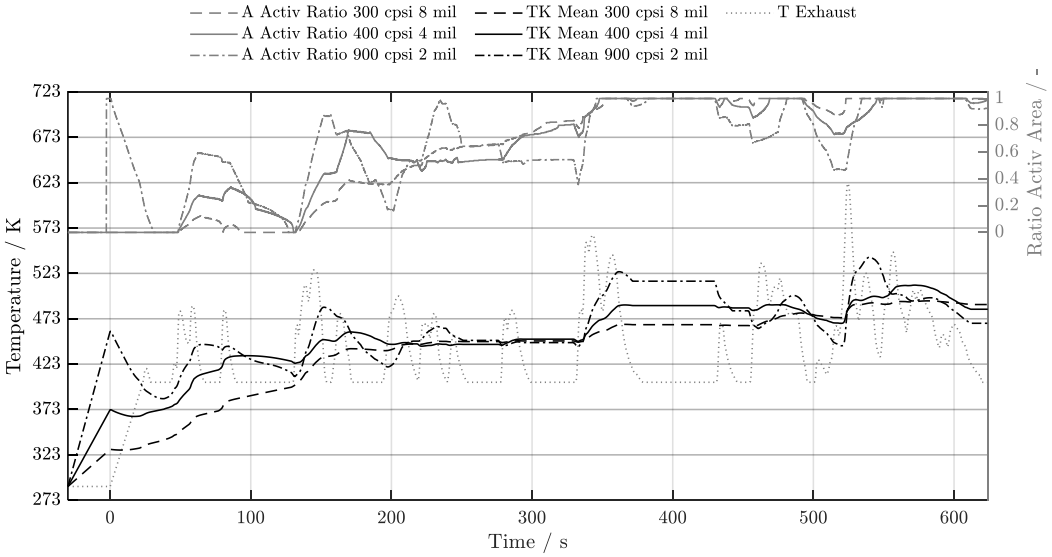

Figure 26. Temperature curve for the case of a 30 s preheat and the cold start scenario w/o start-stop-system.

The 900 cpsi with 2 mil variant is representative of all thin-walled geometries. It has been demonstrated that such materials are capable of withstanding temperature fluctuations with great rapidity, thus facilitating rapid heating. Consequently, the catalytic converter is preheated and at the required temperature when the engine is started. However, the exhaust gas, which is initially cold, rapidly cools the system. This phenomenon severely limits the system's ability to generate any significant benefit. To ensure a sustained advantage, the heating system would need to remain active during the initial cold start phase. While the reference variant does not attain the light-off temperature

 doi:10.20944/preprints202604.1657.v1

prior to engine ignition, it can benefit from the initialization benefit for a considerably longer duration than the high-cell variant. In this case, the advantage is sustained for a considerable duration, extending throughout almost the entire initial half of the cycle. It is evident that the heaviest version attains the lowest temperature level of the three, a consequence of its equivalent preheating power. The body's mass is slightly greater than that of the unheated version due to the incorporation of a hybrid ceramic material.

In summary, the three models have minimal influence on the attainment of the light-off temperature. When the duration of the cycle preceding light-off is considered, the variations are all less than one percent. This finding indicates that the efficiency of preheating with an output of just under 2 kW is negligible in achieving a substantial change in temperature. In order for this technology to be used efficiently, further investigation is required into additional methods, such as the use of electric heating during the engine start-up time. This could prevent the cooling down during the initial phase.

6. Conclusion

The imposition of increasingly stringent emission limits within the transport sector has precipitated the development of sophisticated exhaust gas treatment systems. Over the past decade, the regulatory requirements for all categories of road vehicles have undergone a marked tightening of standards. Consequently, there has been a proliferation of costly systems, which have been developed and implemented. A commonality among these systems is the necessity for elevated thermal levels. The precise temperature level required varies contingent on the catalyst material utilized and the intended function; however, all systems necessitate a distinct light-off temperature.

The oxidation catalyst represents the initial stage in contemporary exhaust gas treatment systems. For stoichiometric petrol engines, this is a three-way catalyst, and for diesel engines, it is a diesel oxidation catalyst. The issue of attaining the requisite temperature is further complicated by the lower exhaust gas temperatures of diesel engines resulting from lean burn operation. The oxidation catalyst is the component within the system that experiences the most significant fluctuations in inlet gas temperature. Consequently, the present study focuses on the thermal behavior of this monoliths due to parameters related to cell density and wall thickness.

The initial segment of this paper pertains to the practical driving test, which was employed to generate the requisite data for the subsequent simulations. A real data test procedure was defined and utilized for the calculation model, following test drives in an urban area. It was deemed essential to utilize a test scenario for the initiation of a cold engine, with the objective of accentuating a primary concern pertinent to mobile ICE applications.

Secondly, all observed geometries were considered on a common basis. In this instance, the contact points between exhaust gas and catalytic converter were standardized to equivalent dimensions. Consequently, the catalytic active area is equivalent for all observed bodies, resulting in uniform conversion rates. Geometric properties such as mass, open frontal area, and the geometric surface area for a widely-used dimension in passenger vehicles—5.66 " in diameter and 6 " in length. The cell densities considered range from 300 cpsi to1200 cpsi, and the wall thicknesses from 2 mil to 8 mil. The selection of combinations for consideration was determined by reference to commercially available monoliths. The 1200 cpsi monolith with 2 mil wall thickness demonstrates the highest heat transfer coefficient and possesses the largest internal surface area, which facilitates the assumption of the fastest response on temperature difference between the honeycomb and the exhaust gas. This is advantageous in terms of rapid heating, but it is also important to note the potential for rapid cooling.

Conversely, the 300 cpsi 8 mil version exhibits the slowest response time, yet it possesses the highest thermal capacity of all the variants. Notably, it was the sole option capable of attaining the requisite light-off temperature under all conditions. The variety of the considered scenarios, even for the same driving profile, brings extreme conditions and different requirements. Consequently, it was not feasible to determine one optimal geometry for all scenarios. Instead, it is crucial to understand the specific requirements of each task and to focus on the most critical ones.

 doi:10.20944/preprints202604.1657.v1

One potential solution that could be considered is the use of a split system, in which a small, light component is responsible for rapid heating, while a heavier component with greater wall thickness is employed to prevent cooling. Furthermore, the subsequent utilization of supplementary options, such as the start-stop system, is of paramount importance. The simulations demonstrated that the impact of engine deactivation during idle phases is effective and a feasible method to prevent the exhaust system from cooling down and enhance the temperature level, independent of the employed geometry of the honeycomb.

Additionally, the potential for supplementary heating from the catalyst was examined. Given the perpetual challenge of spatial constraints in mobile applications, the optimization of space and weight is a paramount consideration for these systems. Consequently, this technique has the potential to achieve a compact, lightweight, and effective emission control system that is both cost-effective and viable. The subsequent years will see a significant focus on material research for this application, with the aim of facilitating the long-term utilization of internal combustion engines (ICE) in mobile applications. This necessitates the customization of materials for specific applications and the development of optimal heating strategies. The development of a heating strategy in conjunction with a thermal isolating system is a particular area of potential efficiency enhancement in the future.

Author Contributions: The author's contributors can be divided into: conceptualization, T.S. and M.W.; development of methodology, T.S. and M.W.; software and modelling, T.S. V.S. and L.N.; validation, T.S., P.P. and L.N.; formal analysis, T.S. M.W. and P.P.; investigation, T.S., P.P. and M.W.; visualization, T.S. M.W.; writing—original draft preparation, T.S. and M.W.; writing—review and editing, L.M. V.S. and C.P.; supervision, L.M., and C.P. All authors have read and agreed to the published version of the manuscript.

Funding: This research received no external funding.

Conflicts of Interest: The authors declare no conflicts of interest..

Abbreviations

The following abbreviations are used in this manuscript:

Latin Letters		
$\boldsymbol{A}$	area	m^2
$\boldsymbol{c_p}$	isobaric heat capacity	$J \cdot kg^{-1} \cdot K^{-1}$
$\boldsymbol{d}$	diameter	m
$\boldsymbol{l}$	length	m
$\boldsymbol{m}$	mass	kg
$\boldsymbol{\dot{m}}$	gravimetric flow rate	$kg \cdot s^{-1}$
$\boldsymbol{Nu}$	Nusselt number	-
$\boldsymbol{p}$	pressure	Pa
$\boldsymbol{Pe}$	Peclet number	-
$\boldsymbol{Pr}$	Prandtl number	-
$\boldsymbol{Q}$	heat	J
$\boldsymbol{\dot{Q}}$	heat flux	W
$\mathbf{R_{sp}}$	specific gas constant	$J \cdot kg^{-1} \cdot K^{-1}$
$\boldsymbol{Re}$	Reynolds number	-
$\boldsymbol{T}$	temperature	K
$\boldsymbol{t}$	time	s
$\boldsymbol{u}$	velocity	$m \cdot s^{-1}$
$\boldsymbol{UI}$	uniformity index	-
$\boldsymbol{V}$	volume	m^3
$\boldsymbol{\dot{V}}$	volumetric flow rate	$m^3 \cdot s^{-1}$
Greek Letters		
$\boldsymbol{\alpha}$	heat transfer coefficient	$W \cdot m^{-2} \cdot K^{-1}$
$\boldsymbol{\Delta}$	difference	-
$\boldsymbol{\lambda}$	heat conductivity	$W \cdot m^{-1} \cdot K^{-1}$
$\boldsymbol{\eta}$	dynamic viscosity	$kg \cdot m^{-1} \cdot s^{-1}$

 doi:10.20944/preprints202604.1657.v1

$\boldsymbol{\rho}$	density	$kg \cdot m^{-3}$
Subscripts		
$\boldsymbol{avg}$	average	
$\boldsymbol{air}$	air	
$\boldsymbol{cat}$	catalytic converter	
$\boldsymbol{c}$	cell	
$\boldsymbol{cond}$	conductive	
$\boldsymbol{conv}$	convective	
$\boldsymbol{exhaust}$	exhaust	
$\boldsymbol{fuel}$	fuel gas	
$\boldsymbol{gas}$	exhaust gas	
$\boldsymbol{hydr}$	hydraulic	
$\boldsymbol{in}$	inflowing	
$\boldsymbol{int}$	internal	
$\boldsymbol{ln}$	logarithmic	
$\boldsymbol{loss}$	heat loss	
$\boldsymbol{light-off}$	light off	
$\boldsymbol{mean}$	mean value	
$\boldsymbol{mono}$	monolith	
$\boldsymbol{open}$	open	
$\boldsymbol{out}$	outflowing	
$\boldsymbol{Ratio\ Activ}$	ratio active area to internal area	
Definitions/Abbreviations		
1D	one-dimensional	
BlmSchV	Bundes-Immissionsschutzverordnung	
C_3H_6	propene	
CO	carbon monoxide	
CO_2	carbon dioxide	
cpsi	cells per square inch	
CxHy	hydrocarbons	
DOC	diesel oxidation catalyst	
EGR	exhaust gas recirculation	
EURO	European emissions standard	
FAQA	Federal Air Quality Act	
GPS	Global Positioning System	
H_2O	water	
HC	hydrocarbons	
ICE	internal combustion engines	
moDiag	motor diagnostic	
NO	nitrogen monoxide	
NO_x	nitrogen oxides	
O_2	oxygen	
OFA	open frontal area	
Pd	palladium	
PM	particulate matter	
Pt	platinum	
RDE	real driving emissions	
Rh	rhodium	
SCR	selective catalytic reduction	
SynAir	synthetic air	
TIER	US emission standard	
TWC	three-way catalytic converter	
USA	United States of America	
WLTP	Worldwide Harmonized Light Vehicles Test Procedure	

 doi:10.20944/preprints202604.1657.v1

Appendix A

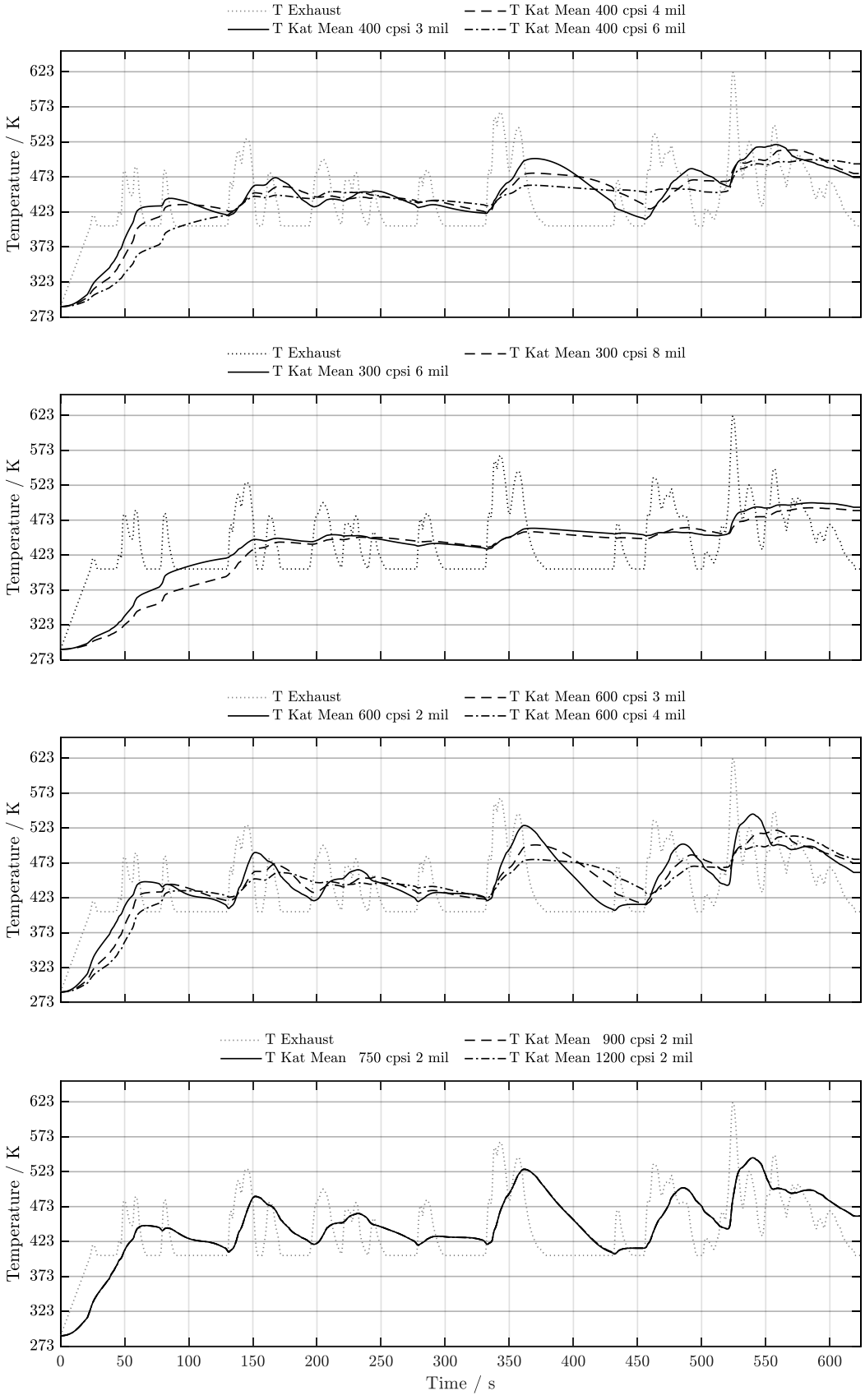

Figure A1. Summary of results for all geometries for cold start w/o start-stop.

 doi:10.20944/preprints202604.1657.v1

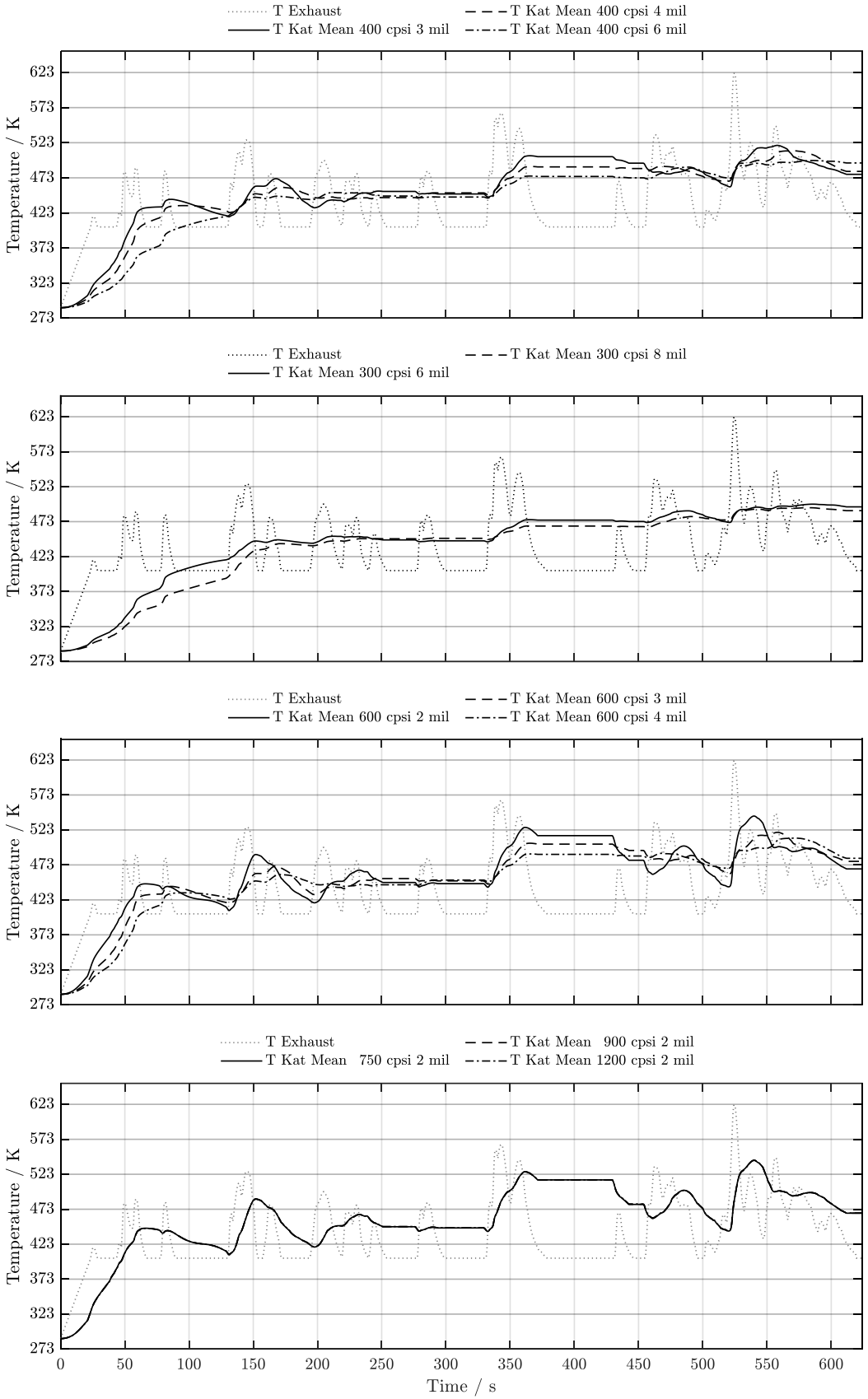

Figure A3. Summary of results for all geometries for cold start w/ start-stop.

 doi:10.20944/preprints202604.1657.v1

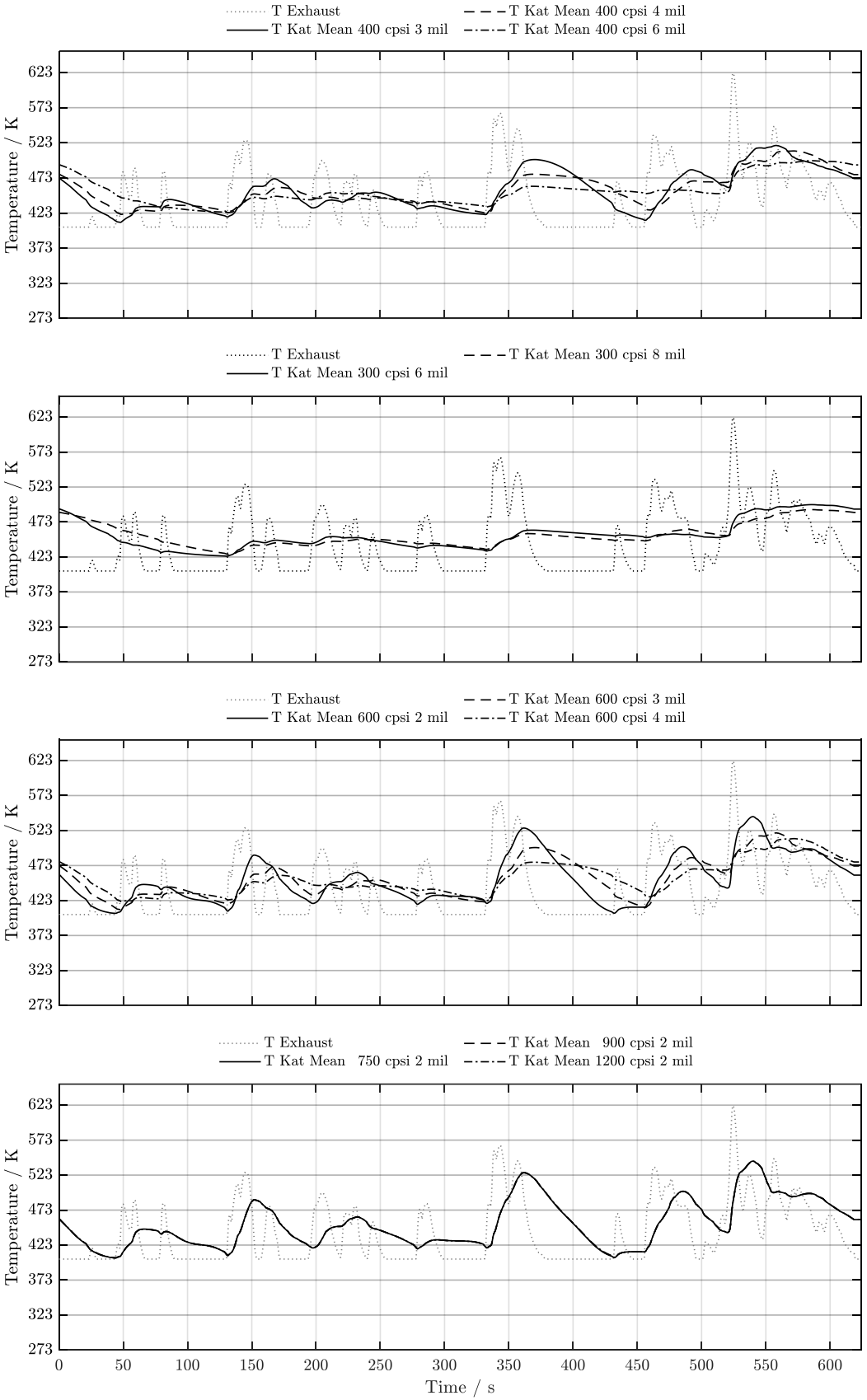

Figure A3. Summary of results for all geometries for warm start w/o start-stop.

 doi:10.20944/preprints202604.1657.v1

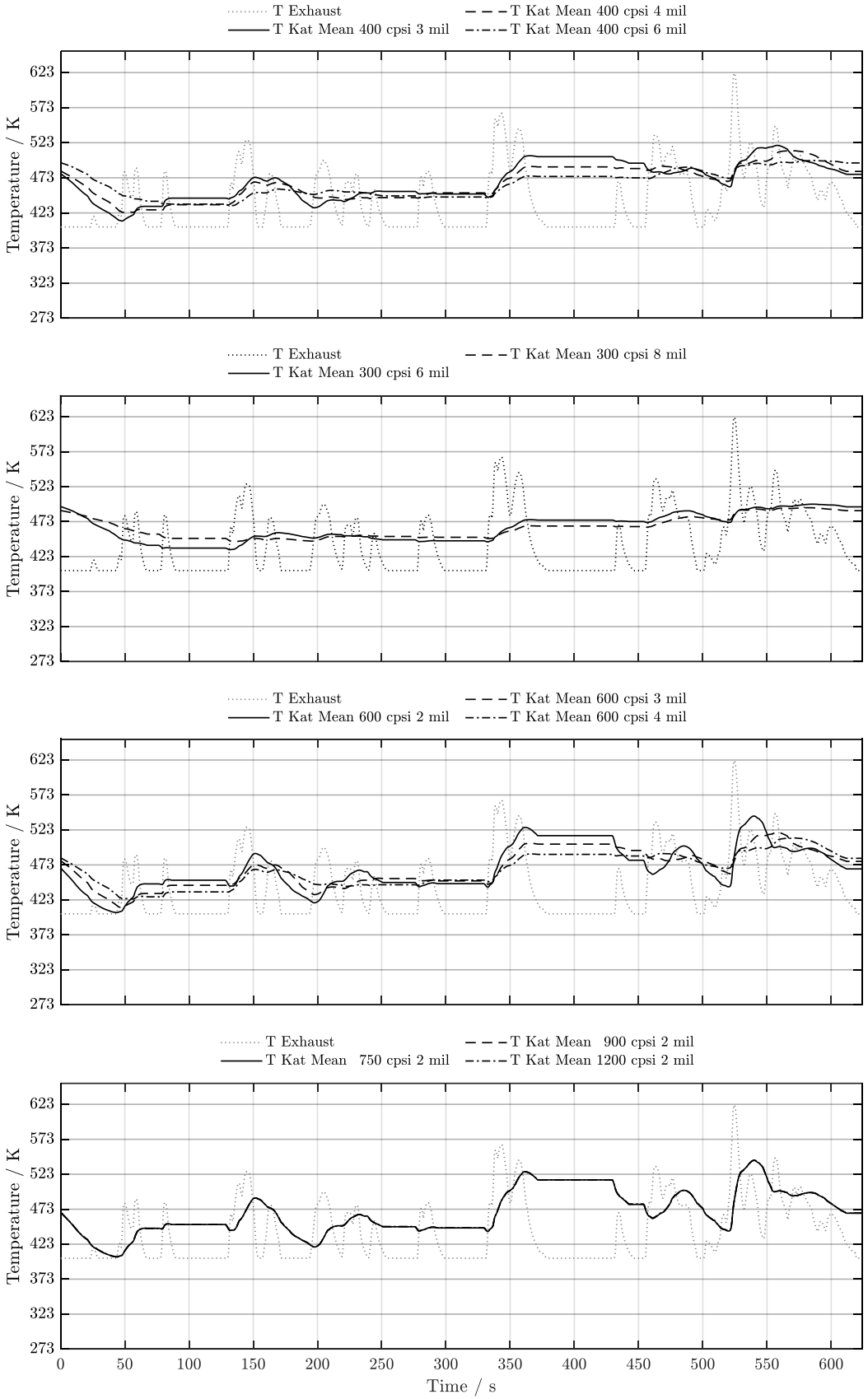

Figure A4. Summary of results for all geometries for warm start w/ start-stop.

 doi:10.20944/preprints202604.1657.v1

References

1. European Commission. Proposal for a Regulation of the European Parliament and of the Council on the Type-Approval of Motor Vehicles and Engines […] (Euro 7). COM(2022) 586 final, Brussels, Belgium, 10 November 2022.
2. U.S. Environmental Protection Agency. Control of Air Pollution From Motor Vehicles: Tier 3 Motor Vehicle Emission and Fuel Standards. Fed. Regist. 2014, 79(57), 16122–16247.
3. U.S. Congress. Federal Air Quality Act of 1967, Public Law 90–148; 81 Stat. 485, 2 November 1967. Available online: https://www.govinfo.gov/content/pkg/STATUTE-81/pdf/STATUTE-81-Pg485.pdf (accessed on [2025.05.05])
4. Bundesministerium des Innern. Erste Verordnung zur Durchführung des Bundes-Immissionsschutzgesetzes (1. BImSchV). Bundesgesetzblatt Teil I 1974, 2121. Available online: https://www.bgbl.de/xaver/bgbl/start.xav?start=//*%5B@attr_id='bgbl174103.pdf'%5D (accessed on [2025.05.05]).
5. Peer, J.; Backes, F.; Sauerland, H.; Härtl, M.; Wachtmeister, G. Development of a High Turbulence, Low Particle Number, High Injection Pressure Gasoline Direct Injection Combustion System. SAE Int. J. Engines 2016, 9, 2301–2311, https://doi.org/10.4271/2016-01-9046.
6. Ming, Z.; Graham, T.R.; Gary, H.J. Diesel engine exhaust gas recirculation—a review on advanced and novel concepts. Energy Convers. Manag. 2004, 45, 883–900, https://doi.org/10.1016/S0196-8904(03)00194-8.
7. Bin, C.; Li, Z.; Jinlin, H.; Qing, Z. A combination of electric supercharger and Miller Cycle in a gasoline engine to improve thermal efficiency without performance degradation. Case Stud. Therm. Eng. 2019, 14, 100429, https://doi.org/10.1016/j.csite.2019.100429.
8. Marsh, P.; Acke, F.; Konieczny, R.; Brück, R.; Hirth, P. Application Guideline to Define Catalyst Layout for Maximum Catalytic Efficiency. In SAE 2001 World Congress, Detroit, MI, USA, 5–8 March 2001; SAE International, 2001.
9. Steiner, T.; Neurauter, D.; Moewius, P.; Pfeifer, C.; Schallhart, V.; Moeltner, L. Heat-Up Performance of Catalyst Carriers—A Parameter Study and Thermodynamic Analysis. Energies 2021, 14, 964, https://doi.org/10.3390/en14040964.
10. Brück, R. Neue Katalysatorträger-Innovation für RDE- und SULEV-30-Grenzwerte. MTZ 2016, 78, 18–27, https://doi.org/10.1007/s35146-016-0163-8.
11. Harth, G. Intelligente Katalysatorentechnologien für zukünftige Emissionsanforderungen. In 32. Internationales Wiener Motorensymposium, 5.–6. Mai 2011; Lenz, H.-P., Ed.; VDI Verlag GmbH: Düsseldorf, Germany, 2011; pp. 246–257. ISBN 978-3-18-373512-9.
12. Möltner, L.; Schallhart, V.; Berthold, H. Silikatkeramischer Kompositwerkstoff und Anwendungen davon. Austrian Patent A 50628/2021, 30 July 2021.
13. Nieken, U.; Eigenberger, G.; Tuttlies, U.S.; Bernnat, J. Katalytischer Brenner für ein wärmeintegriertes Motorabgasreinigungssystem; Universitätsbibliothek der Universität Stuttgart: Stuttgart, Germany, 2009.
14. Hudec, J.; Šarkan, B.; Cződörová, R., Examination of the results of the vehicles technical inspections in relation to the average age of vehicles in selected EU states, Transportation Research Procedia. 55. 2-9. 10.1016/j.trpro.2021.07.063
15. Landeshauptstadt Innsbruck, City-Map Innsbruck. Available online: https://city-map.innsbruck.gv.at/stadtplan/client_workspace/FatalError.jsp;jsessionid=D5D860C04CCB6987F2D5BF6FF01D6775?synergis_session=02d2ef88-5742-4502-bf69-7e581dc57f08&tsp=1746781930310 (accessed on [2025.09.09]).
16. Moeltner, L.; Hohensinner, M.; Schallhart, V. Experimental and Numerical Analysis of Low Temperature NOx Conversion in Urban Busses. In SAE 2016 Commercial Vehicle Engineering Congress; SAE International, 2016.
17. Moore, W.J. Physikalische Chemie; De Gruyter: Berlin, Germany, 1986; ISBN 978-3-11-010979-5.
18. Kleiber, M.; Joh, R. VDI-Wärmeatlas; Verein Deutscher Ingenieure (VDI-GVC): Berlin, Germany, 2006; ISBN 978-3-540-25504-8.

 doi:10.20944/preprints202604.1657.v1

19. Wishart, J.; Shirk, M.; Gray, T.; Fengler, N. Quantifying the Effects of Idle-Stop Systems on Fuel Economy in Light-Duty Passenger Vehicles. In SAE 2012 World Congress & Exhibition; SAE International, 2012.
20. Statistisches Bundesamt, Erwärbstätigkeit – Berufspendler. Available online: https://www.destatis.de/DE/Themen/Arbeit/Arbeitsmarkt/Erwerbstaetigkeit/Tabellen/pendler1.html (accessed on [2025.09.15]).